Journal of Controlled Release 314 (2019) 125–140

Contents lists available at ScienceDirect

Journal of Controlled Release

journal homepage: www.elsevier.com/locate/jconrel

Review article

Nanoparticle-mediated approaches for Alzheimer's disease pathogenesis, diagnosis, and therapeutics

Sajini D. Hettiarachchi[a], Yiqun Zhou[a], Elif Seven[a], Madepalli K. Lakshmana[b], Ajeet K. Kaushik[c], Hitendra S. Chand[b], Roger M. Leblanc[a,*]

[a] Department of Chemistry, University of Miami, 1301 Memorial Drive, Coral Gables, FL, 33146, USA
[b] Department of Immunology and Nano-Medicine, Herbert Wertheim College of Medicine, Florida International University, 11200 SW 8th Street, Miami, FL 33199, USA
[c] Department of Natural Sciences, Division of Sciences, Arts & Mathematics, Florida Polytechnic University, Lakeland, FL 33805-8531, USA

ARTICLE INFO

Keywords:
Alzheimer's disease
Nanoparticles
Amyloid β
Acetylcholine
ROS
Tau protein

ABSTRACT

Alzheimer's disease (AD) is an irreversible and progressive neurodegenerative disorder manifested by memory loss and cognitive impairment. Deposition of the amyloid β plaques has been identified as the most common AD pathology; however, the excessive accumulation of phosphorylated or total tau proteins, reactive oxygen species, and higher acetylcholinesterase activity are also strongly associated with Alzheimer's dementia. Several therapeutic approaches targeting these pathogenic mechanisms have failed in clinical or preclinical trials, partly due to the limited bioavailability, poor cell, and blood-brain barrier penetration, and low drug half-life of current regimens. The nanoparticles (NPs)-mediated drug delivery systems improve drug solubility and bioavailability, thus renders as superior alternatives. Moreover, NPs-mediated approaches facilitate multiple drug loading and targeted drug delivery, thereby increasing drug efficacy. However, certain NPs can cause acute toxicity damaging cellular and tissue architecture, therefore, NP material should be carefully selected. In this review, we summarize the recent NPs-mediated studies that exploit various pathologic mechanisms of AD by labeling, identifying, and treating the affected brain pathologies. The disadvantages of the select NP-based deliveries and the future aspects will also be discussed.

1. Introduction

Alzheimer's disease (AD) is an irreversible neurodegenerative disorder of the elderly characterized by progressive intellectual deterioration involving memory, language, and judgment, ultimately leading to total dependence on nursing care. More than 100 million people worldwide will be living with dementia by 2050 [1], with an estimated cost to reach 1 trillion by next year [2]. AD is the leading cause of dementia, and the possibility of developing AD roughly doubles every five years after 65, and it is close to 50% over the age of 85 [3,4]. The major hallmark features of AD include the extracellular deposition of beta-amyloid (Aβ) plaques, the intraneuronal accumulation of neurofibrillary tangles (NFT) due to hyperphosphorylated tau, loss of synapses and neurons, vascular abnormalities, glial dysfunctions and neuroinflammation [5–8]. Although plaques and tangles are the major constituents in AD, there is no compelling evidence that the neurodegenerative process in AD begins in synapses. For example, the extent of synaptic loss, which begins prior to the appearance of tangles, plaques, or neuronal loss is an excellent correlate of dementia [9–11]. While the mechanism of neuropathology and the genetic basis of familial cases of AD (FAD) have been fairly understood, the molecular basis for sporadic cases of late-onset-AD (LOAD) which comprises the majority cases of AD is far from clear. Inheritance of two apolipoprotein E (APOE) ε4 alleles (APOE ε4/ε4) is the single most significant genetic risk factor for the development of LOAD [12], and sixty percent of all AD patients carry at least one APOE ε4 allele [13]. More recent studies have identified a large number of other genetic risk alleles [14–16], implying that AD is a complex and highly heterogeneous disease.

Amyloid plaques are parenchymal deposits of Aβ, a fibrillous 4-kDa protein of 40 to 43 amino acids derived from amyloid precursor protein (APP) by the sequential actions of β- and γ-secretases at the N- and C-terminus of the Aβ domain, respectively [17]. FAD mutations are known to increase the generation of Aβ or produce more aggregation-prone Aβ. The oligomerization of excess Aβ leads to the plaque formation that causes neuronal cell death via intracellular neurofibrillary tangle formation and synaptic dysfunction leading to the loss of cognitive functions [5–11].

The abnormal hyperphosphorylation of a microtubule-associated tau protein (P-tau) has also been implicated in the AD pathogenesis. The P-tau proteins produce neurofibrillary tangles, neuropil threads,

* Corresponding author.

https://doi.org/10.1016/j.jconrel.2019.10.034
Received 22 July 2019; Received in revised form 16 October 2019; Accepted 18 October 2019
Available online 21 October 2019
0168-3659/

and neurotic plaques, which are surrounded by dystrophic neurites, that lead to AD development [18]. The elevated levels of both Aβ-42 and P-tau proteins in cerebrospinal fluid (CSF) are two excellent biomarkers that distinguish AD from other neurodegenerative diseases. Tau protein is phosphorylated either at threonine 231 (P-tau$_{231P}$) or serine 199 (P-tau$_{199P}$), with P-tau$_{231P}$ being the dominant form associated with the higher risk of Alzheimer's dementia [19].

Acetylcholine (ACh) is an essential neurotransmitter in the central and peripheral nervous systems. The elevated levels of acetylcholinesterase (AChE) reduce the ACh concentration and contribute to AD. There are several regions in the brain, including basal forebrain, where the cholinergic neurons are innervated [20]. The loss or degeneration of the cholinergic neurons in the basal forebrain, strongly intercorrelate with Aβ deposition and plaque formation, at the early stages of AD. The upregulation of AChE in mild AD condition does not affect the cholinergic forebrain neurons, but the loss of calcium-binding proteins (calbindin) in basal cholinergic forebrain induces the formation of tangles and severe functional alterations in cholinergic neurons. The severe functional impairment in the cholinergic neuronal axon reduces the neurotransmitter ACh and its biosynthetic enzyme choline acetyltransferase or ChAT [21]. There is a strong correlation between the AChE levels and the amyloid tangle formation. Therefore, blocking AChE activity has been proposed as one of the strategies to treat the cognitive impairment of AD patients.

The neurotoxic accumulation of reactive oxygen species (ROS) has also been identified as a possible pathogenic mechanism for AD development. ROS, such as hydrogen peroxide, superoxide anions, and hydroxyl radicals, cause mitochondrial dysfunction, and cell death [22–24]. The brain consumes 20% more oxygen than any other tissue, which makes it more susceptible to the potential damage by ROS. The APP is expressed in higher quantities when the brain attempts to repair the oxidative damage caused by ROS, which in the case of AD, leads to the production and accumulation of Aβ plaques [25–27]. This leads to a higher production of superoxide anions, which diminishes the oxidative phosphorylation and the cellular ATP pool causing mitochondrial dysfunction and further development and severity of AD.

Numerous treatment modalities and therapeutics have been developed to target the above-described AD pathologies, i.e., Aβ aggregation, P-tau protein, ROS, and AChE inhibitions [28,29]. Recent studies have proposed the utility of tacrine, estradiol, curcumin, and peptides, including D-peptide in AD treatment [30–33]. However, the above potential therapeutics have been limited due to the poor permeability of the blood-brain barrier (BBB) and side effects of subacute myelopathic neuropathy (SMON) [22,34]. Nano-delivery is a superior alternative due to the site-specific delivery, ability to cross the BBB, enhanced drug solubility, and higher therapeutic efficacy. Nanoparticles (NPs) used for drug encapsulation, which increases the drug half-life and sustained-release while extending further bioavailability in the brain [35,36]. The capacity of multiple drug loading onto NPs also improves the therapeutic efficacy. Furthermore, the ability to tag a site-specific ligand enhances the accumulation of drugs at the specific tissue region and the drugs' ability to cross the BBB [37–39]. NPs thus play a significant role in providing better treatment options for AD, and this review discusses the different types of NPs which have been exploited to develop the AD treatments in the field of targeted drug delivery.

2. Nanoparticles

NPs are materials that lay on the 1–100 nm scale. The numerous organic and inorganic materials can be used to synthesize NPs. NPs are popular as nanocarriers, mainly due to their characteristics such as high water dispersity, biocompatibility, and biodegradability [40–42]. Most of the drugs that target AD have low bioavailability and lack of ability to cross BBB. Therefore, NPs are mostly the best candidates to deliver drugs to the brain that can improve the drugs' bioavailability and half-life even at a lower concentration. NPs also enhance the efficacy of therapeutics by increasing the target specificity, via reducing the acute toxicity [43–45]. There are varieties of nanoparticles that have been used in AD studies. The most popular nano-agents are liposomal and polymeric NPs, while metallic, carbon-based, and curcumin NPs have also been studied. Therefore, this review article focuses on NPs' participation in different pathogenesis of AD (Table 1).

2.1. Liposomal NPs

Liposomal NPs were introduced in 1965, which was the first NP used as a nano-drug carrier. Liposomes are spherical-shaped vesicles which have an aqueous inner core and vesicle shell. They consist of the single or bilayered lipid membrane structure [46,47]. The amphiphilicity of the phospholipid molecules in lipid vesicles make liposomes amphiphilic. The impressing fact is, not all the lipid or phospholipid combinations in the nanoscale make liposomes. Some nano-scale phospholipids combinations have different shapes, such as hexagonal, micellar, or cubic phases, making them deviate from the liposomal characteristics, wherein only the vesicle spheres have the liposomal NPs features [48]. Liposomes are highly biodegradable, non-toxic, and non-immunogenic [47,49]. The size distribution of liposomal NPs is broad as 10 nm – 10 μm. Liposomal NPs can encapsulate hydrophilic agents in their hydrophilic cores and hydrophobic agents in their hydrophobic membranes. The versatile structure of liposomal NPs makes them easy to load probes and therapeutic agents, which also facilitate BBB penetration. Liposomal NPs can be synthesized by using many different natural sources such as milk, soy, eggs, and even the very first natural food, breast milk [50–52]. These natural sources are enriched with phospholipids and lipid vesicles, which provide liver protection and memory improvement as health welfares to liposomal NPs [53–55]. Therefore, liposomal NPs are one of the best candidates to be used in AD drug delivery systems.

Due to the broadness of AD, liposomes have been applied to target numerous AD pathogenesis. Masserini and co-workers have designed amphipathic liposomal NPs, to target the gangliosides of the Alzheimer's brain while showed a higher affinity to A$\beta_{1\text{-}42}$ peptide and lysosomes [56–58]. Liposomal NPs were made up of a 1:1 molar ratio of sphingomyelin (Sm) and cholesterol mixed with and without 5 or 20% of one of the following lipids; gangliosides, Sm, 1-palmitoyl-oleoyl-phosphatidylcholine (PC), phosphatidylethanolamine (PE), phosphatidylglycerol (PG), dimyristoylphosphatidic acid (PA), or cholesterol lipids (CL). The particle sizes of all the combination types of liposomes were approximately 144 − 178 nm and the zeta potentials were −11 to −50 mV. The excellent stability of liposomal NPs and the consistency of their size over time up to 48 h were confirmed by dynamic light scattering (DLS). The binding of liposomes to commercially or lab synthesized A$\beta_{1\text{-}42}$ was investigated by surface plasmon resonance (SPR). Even though the SPR results suggested that the PA, CL, and ganglioside liposomes showed the best affinity towards A$\beta_{1\text{-}42}$, the results have not been further proved by *in vivo* or *in vitro* studies [56]. Authors have also confirmed the cell-permeability of their large size liposomal NPs by using those as bio-imaging probes that are conjugated with cell-permeant dye calcein. The conjugated system displayed green fluorescence due to the acetoxymethyl ester hydrolysis after the interaction with intracellular esterases, which proved the successful cell membrane penetration of the liposomal conjugated system [56]. However, the authors suggested that their results are open to the public to develop better nanocarrier for imaging and drug delivery in AD studies. Therefore, based on the above research, Balducci et al. designed a receptor-mediated liposomal model of bifunctionalized liposome, mApoE-PA-Lip, by using mApoE peptide (which derived from apolipoprotein-E) and phosphatidic acid (PA) [59]. The mApoE peptide is the BBB binding ligand, and phosphatidic acid directs the NP system to Aβ binding domain. The overall particle size after the conjugation was approximately 120 nm and the zeta potential was -18.7 mV. The *in vitro* studies were conducted with synthetic A$\beta_{1\text{-}42}$ fibrils in phosphate buffer

Table 1
Representative nanoparticles used for AD-related studies.

NPs Type	Particle Size (nm)	Structure	Characteristics	Mostly targeted AD Pathogeneses	Popular Drugs/genes/ peptides/small molecules	*In vitro* cell lines	*In vivo* mouse models	References
Liposomal NPs	10 -10 000	Spherical-shaped vesicles contain an aqueous inner core and vesicle shell	Non-toxicity, Non-immunogenicity, Bio-degradability	Aβ cascade, Cholinergic dysfunction	mApoE, H102, XO4, ET621	calu-3	APP/presenilin 1, APP23	[46–64]
Chitosan NPs	< 70	Natural starch cationic polysaccharide composed of two co-polymers of glucosamine and *N*-acetylglucosamine	Bio-compatibility, Bio-degradability, Non-lethality, Low immunogenicity, Higher surface to volume ratio, Higher degradation tendency	Cholinergic dysfunction	Tacrine, GH, Piperine	N/A	5XFAD SDAT	[69–83]
Synthetic polymeric NPs	100-300	Colloidal particles of PLGA, PEG	High solubility, permeability, and loading capacity. Low toxicity	Aβ cascade, Tau protein phosphorylation, Endogenous estrogen deficiency	Estradiol, RVG29, D-peptide, siRNA, shRNA	bEnd.3	C57BL/6 J	[37,67,84–97]
Gold NPs	1–100	Metal-based NPs made up of Au^{3+}. Wine red color in the colloidal solution.	Low cytotoxicity, and Size-dependent optical properties. Colorimetric sensors.	Metal-ion interaction with Aβ, Tau protein phosphorylation, Cholinergic disfunction	Tau-mab	N/A	N/A	[101–116]
Magnetic NPs	< 70	Metal-based NPs mostly made up of iron, copper, and zinc.	Metal-ion chelators	Aβ cascade, Tau protéine phosphorylation, ROS inhibition	TPP	PC12, SH-SY5Y	5XFAD	[23,24,117–137]
Carbon nanotubes	1-100	Fullerene allotropes consist of the long cylindrical shaped hollow structure.	High in thermal conductivity, optical, and electrical properties. High cell penetration. Toxic to human keratinocytes, kidney cells, T lymphocytes, and alveolar macrophages.	Aβ cascade, Cross β stacking, Cholinergic dysfunction, ROS inhibition	Ach	N/A	CRND8	[140–153]
Carbon Dots	1–10	Spherical shaped zero-dimensional nanostructures with tunable surface functionalities	High photoluminescence intensity, bio-compatibility, and cell permeability. Excitation wavelength-dependent/independent emission, and tunable surface. Nontoxicity	Aβ cascade, Cholinergic dysfunction	Transferrin	N/A	N/A	[39,154–165]
Curcumin NPs	< 100	Made up from an Indian and Chinese spice, *Curcuma longa*	Polyphenolic antioxidant, ROS scavenger	Aβ Cascade, Tau protein phosphorylation	N/A	MDCK	Tg2576	[35,166–175]

solution. The electron microscopic images have shown the ability of liposome conjugate to disaggregate and delay the formation of Aβ deposits. The *in vivo* studies were performed by 10 months old APP/presenilin 1 transgenic mice (Fig. 1). The mice were injected with mApoE-PA-LIP for three times (once a week) before the histological analysis. The results have displayed, the reduction of brain soluble $A\beta_{1\text{-}42}$ by 33% and the total plaques by 34%. The PET imaging studies conducted with APP23 mice have revealed the depletion of Aβ deposits after the treatments of bifunctionalized liposomes, mApoE-PA-LIP. Therefore, the authors concluded saying the mApoE-PA-LIP showed the superiority by crossing BBB, interacting with the AD brain region, and diminishing the Aβ aggregates. The depletion of Aβ was stable for more than 3 months of period (Fig. 2).

Due to the successfulness of the mApoE-PA-LIP conjugates, it has been repeatedly used in AD studies in recent years. The peripheral sink effect and withdrawal of Aβ peptide from different aggregation forms of the brain have been studied by Mancini et al. in 2016 by using a transwell cellular model of the BBB for *in vitro* study and APP/PS1 mice for *in vivo* study [60]. Mancini et al. used the same liposome conjugation (mApoE-PA-LIP), as Balducci *et al.* studied [59,60]. The mApoE-PA-LIP that synthesized by Mancini et al. was approximately 140 nm in size and has −18.32 mV of zeta potential [60]. The principal goal of their study is to identify the type of Aβ that capable of crossing the endothelial cells in the transwell BBB model to be in the equilibrium of the brain and blood side. Their control experiment stated that only the small soluble Aβ oligomers spontaneously crossed the endothelial monolayer, but not the Aβ fibrils. In the presence of liposomal conjugation of mApoE-PA-LIP, the concentration of Aβ oligomers was enhanced 5-fold in the apical compartment (which mimics the blood side) in the transwell model compared to the basolateral compartment (which mimics the brain side). Authors verified the higher permeability of Aβ oligomers into the blood is due to the higher binding affinity of Aβ oligomers with mApoE-PA-LIP. However, the authors are not capable of ascertaining the permeability of Aβ fibrils from the brain side to the blood side by their transwell model.

In addition to PA and apolipoprotein-E peptides, Aβ targeting fluorescent lipid, 1,2-distearoyl-*sn*-glycero-3-phosphoethanolamine-*N*-[methoxy-XO4-(polyethylene glycol-3400)] sodium salt (DSPE-PEG_{3400}-XO4) conjugated stealth liposomes were synthesized by Tanifum et al. in another liposomal Aβ targeting study [61]. The symmetrically shaped methoxy XO4 group in the lipid conjugation works as the binding ligand to Aβ moiety and the fluorescent marker (Fig. 3). Tanifum et al. tested the binding ability of lipid conjugated liposomes with synthetic Aβ fibrils and then the selectivity of finding the Aβ deposits by the conjugated system in AD transgenic mouse brain tissues [61]. Aβ deposits have many binding sites that can be targeted by structurally different small-molecule ligands [62]. Congo red, Chrysamine G (CG), Thioflavin T, and their derivatives are the most common dyes used to identify the amyloid binding pockets. Therefore, based on the above fact, Tanifum et al. stated both DSPE-PEG-XO4 (NPs bound XO4) and free XO4 bind to the same binding pocket as where CG binds. Also, the authors further confirmed that the NPs bound XO4 showed a longer retention time in the brain compared to free XO4 [61]. The *ex vivo* studies have been conducted by an intravenous tail injection to 12-month-old APP/PSEN1 transgenic mice. After 72 h, mice were sacrificed, and their brain sections were analyzed by confocal microscopy. Rhodamine was encapsulated into liposomes to screen the amyloid plaques and confirmed the intact of liposomal structure. Even though this study does not mention the particle size of DSPE-PEG-XO4, all the *in vitro* immunohistochemistry, *in vivo,* and *ex vivo* studies confirmed the ability of the liposomal NPs to cross the BBB and bind Aβ plaques. However, later, in 2016, Tanifum et al. conversely reported that methoxy-XO4 liposomes were hydrophobic, which also interfere with the lipid bilayer formulation [63]. Thus, XO4-targeted liposomes were mostly unstable in magnetic resonance imaging (MRI) when Gd chelates interact with XO4 bound liposomal systems. Therefore, even

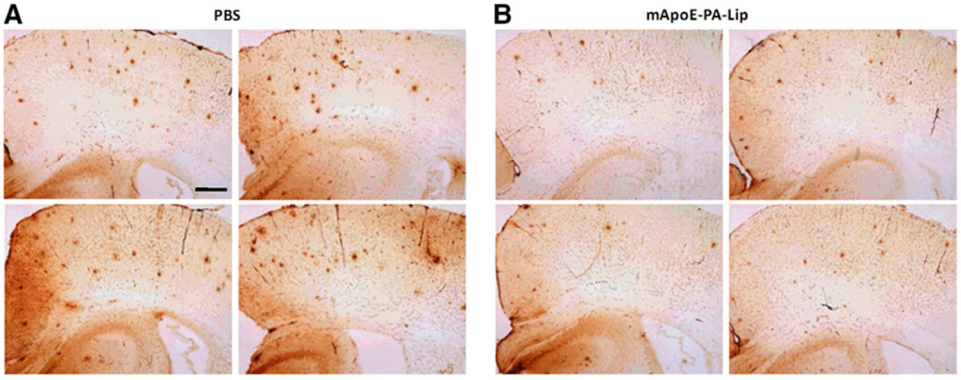

Fig. 1. The PET images of the $A\beta_{1-42}$ plaques in APP/PS1 transgenic (Tg) mice. A) Cortical and hippocampal brain sections of mice treated with PBS B) Cortical and hippocampal brain sections treated with mApoE-PA-LIP. Figure reproduced from Ref. [59] with permissions from the publishers.

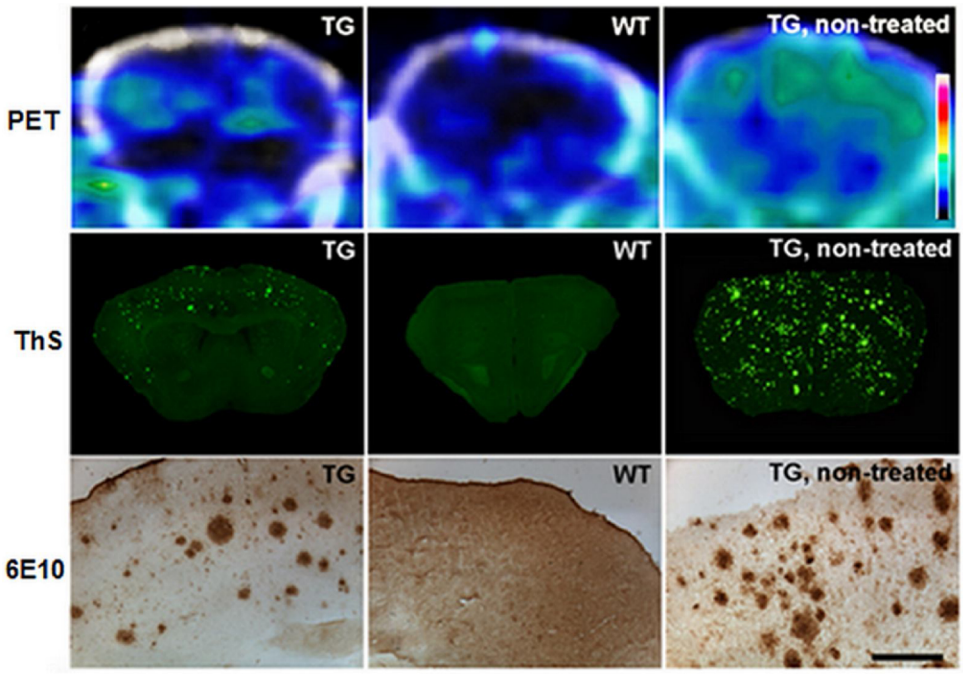

Fig. 2. The PET images of the Aβ plaque depletion in APP23 Tg and WT mice, after the treatments with bifunctinalized, mApoE-PA-LIP compared to non-treated Tg mice. The cortical sections' Aβ binding pockets were stained by Thioflavin-S (ThS) or 6E10 anti-Aβ-antibody (6E10). Scale bar represents 200 μm. Figure adapted from Ref. [59] with permissions from the publishers.

though the methoxy-XO4 capable of penetrating BBB, it is failed in the MRI process. The authors suggested this instability might be due to the osmotic gradient that occurred by the high internal concentration of Gd chelates. Therefore, they have further modified the methoxy-XO4 to synthesize less hydrophobic analogs such as ET6-21. The new candidate, ET6-21, has shown the capability of successful Gd encapsulation into liposomal NPs core while maintaining the stable hyper-relaxive surface of Gd chelates in the lipid bilayer that facilitates the MRI.

Zheng et al. introduced H102 (HKQLPFFEED) peptide-loaded liposomes to deliver drugs for the AD treatments [64]. The mean particle size of the peptide loaded-liposomes was 112.2 nm with a narrow distribution range. The zeta potential was -2.96 mV, and the peptide loading ability on liposomes was 71.35%. The secondary structure formation of the peptide was analyzed by circular dichroism (CD) concerning free H102. The α-helix and β-sheet formation of the free H102 peptide was 15.46 and 9.16%, respectively, while the liposome bound-H102 peptide displayed 8.15 and 14.08%, respectively. The authors suggested the creation of β-sheets in the conjugated model leads to confine the peptide into a small volume that increases cell penetration. The *in vitro* studies have been performed with human bronchial epithelium cell lines of calu-3. The calu-3 cell lines were used as the nasal platform to investigate the nasal membrane penetration of the liposome-peptide conjugate. H102 conjugated liposomal NPs have crossed the calu-3 cell monolayer by mimicking the efficiency of nasal membrane penetration. Authors stated that the liposome bound H102 showed lower absorption rate and longer retention time compared to free H102, suggesting liposome bound H102 as a superior candidate to deliver drugs. The brain uptake study further proved that no drug was found in the brain after the intravenous administration of the liposome bound H102, verifying the incapability of BBB penetration. The intranasal administration has shown a better absorption in the brains' olfactory bulb region, proving the intranasal administration is the best method to deliver drugs with H102 bound liposomes. Moreover, the authors reported that the liposomal bound H102 and free H102 could protect the central cholinergic neurons, by reducing the AchE levels and enhancing the ChAT to upregulate the ACh secretion to diminish the cognitive impairment.

2.2. Polymeric NPs

Polymeric NPs fall into two categories, such as natural and synthetic NPs. Chitosan and cellulose-based polymeric NPs are the natural formers, while synthetic polymeric NPs are usually made up of binding copolymers into another polymer matrix [65]. Chemical synthesis of

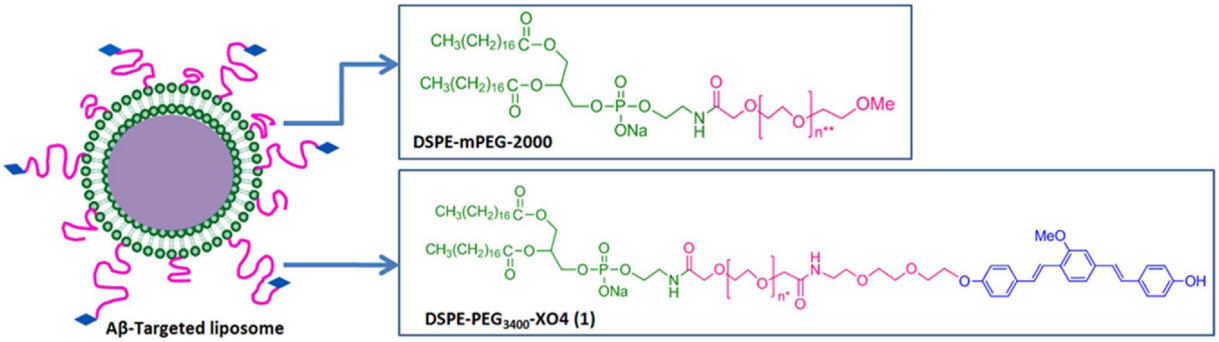

Fig. 3. Lipid conjugated stealth liposome. Figure reproduced from Ref. [61] with permissions from the publishers.

polymeric NPs can be achieved by emulsification, salting out, and nanoprecipitation [66,67]. The particle sizes of chitosan and synthetic polymers range from 50 to a few hundred nanometers. Drugs or any ligands can be loaded onto polymeric NPs by chemical conjugation, surface adsorption, or encapsulation [68].

2.2.1. Natural polymeric NPs - chitosan

Chitosan is a natural starch and cationic polysaccharide composed of glucosamine and *N*-acetylglucosamine copolymers [69]. It is a deacetylation type of chitin obtain from crustacean shells such as lobster, crab, or shrimp. Chitosan can be hydrolyzed into its non-carcinogenic, non-toxic, and non-immunogenetic amine sugar products by the enzyme, lysozyme, that can be further absorbed and degraded by the human body; thus, chitosan is a biodegradable NP [70]. Chitosan acts as self-medication, downregulating cholesterol, and facilitating anti-ulcer activity and wound healing. Chitosan has been approved by the FDA for wound dressings. The application of chitosan NPs for biomedical applications has recently become a favored field, because of the biocompatibility, biodegradability, nonlethal, and low immunogenicity [71]. Chitosan NPs have particle sizes less than 70 nm, which shows a higher surface to volume ratio. According to the literature, the drug encapsulation efficiency of chitosan increases with molecular weight reduction [72]. However, literature studies have further stated that the degradation tendency of chitosan also increases with molecular weight reduction [73]. The chitosan nano-deliveries are used mostly used in oncology studies, but limited in neurodegenerative targeted deliveries [74,75].

Apart from the most common AD hypothesis of Aβ cascade, the cholinergic system abnormality also plays a vital role in AD brains. Chitosan-based AD-related drug deliveries have mostly targeted the cholinergic system by loading some popular drugs such as tacrine and galantamine hydrobromide. Cholinergic dysfunction leads to central memory impairment in AD patients [76]. Therefore, the restoration of cholinergic neurotransmission by inhibiting cholinesterase via increasing the acetylcholine (Ach) concentration in the AD brain will be a remarkable treatment to recover cognitive failure. Tacrine was the first acetylcholinesterase inhibitor, which reversibly inhibits AChE. However, later studies discovered tacrine is a potent reversible inhibitor for butyrylcholinesterase rather than acetylcholinesterase [77]. The bioavailability of tacrine is as low as 17%, which shows the need of a nanocarrier to increase the bioavailability. Wilson et al. have synthesized tacrine-containing chitosan NPs to increase the bioavailability of tacrine [78]. The spontaneous emulsification method was used to bind tacrine with chitosan gel. The average particle size was 41 nm after the drug loading, and the drug loading capacity was approximately 15%. The *in vitro* drug release ability was tested by the dialysis method, whereas the sustained drug release was observed for 12 h. The accumulative, drug release was higher from the NPs that have a higher loaded percentage of drugs, and polysorbate 80 coated tacrine loaded chitosan NPs showed a sustained drug release of 83–94%. Moreover, this study discovered the higher tacrine concentration in the liver, spleen, and lung when intravenously injected with NPs compared to free drug administration. The authors suggested that the observed higher tacrine concentration in organs when tacrine is bound to NPs was due to the dual uptake by the normal blood circulation through organs and the NP uptake by the reticuloendothelial system. However, the above study does not discuss brain uptake studies; instead, the authors mentioned the glazing of the NPs by hydrophilic polymer surfactants favor the dysopzonization, which can be facilitated the reduction of reticuloendothelial system uptake to the liver, which ultimately causes to increase the NP brain uptake [78].

In another study, piperine-loaded chitosan NPs were fabricated by Elnaggar et al. [79]. The chitosan NPs synthesized in this study have an average size of 230 nm after piperine was loaded. The *in vitro* piperine release study performed by dialysis (for 2 h), confirmed that the controlled release of piperine in piperine-loaded chitosan NPs was higher than unbound piperine. *In vivo* studies have also been conducted with an animal model of senile dementia of Alzheimer type (SDAT); which is a model to study the colchicine-induced cognitive dysfunction. In AD brains, colchicine increases the generation of free radicals, which causes to increase the AChE secretion. The elevated level of AChE reduces the Ach concentration in the brain, which causes to increase the cognitive impairment [76]. Therefore, Elnaggar et al. stated, based on the results of *in vivo* studies, that the reduction of Ach concentration by colchicine could be restored by piperine loaded chitosan NPs, making them a good candidate to reduce the cognitive dysfunction in AD brain [79].

Galantamine hydrobromide (GH) is a reversible competitive inhibitor for AChE. It binds to nicotinic acetylcholine receptor allosterically to increase the receptors' sensitivity to Ach [80]. GH also been identified as a drug to slow down plaque formation and the behavioral decline in 5XFAD mice [81]. However, the clinical trials have shown that the oral administration of GH in AD patients has given adverse side effects on organelles, showing the need for an alternative method to deliver GH to the brain [82]. Hanafy et al. in 2016 reported a reaction between GH and chitosan complex NPs to synthesize CX-NP2 NPs, to compare the pharmacological and toxicological profile of free GH and chitosan bound GH [83]. The AChE level and activity in the rat brain have been studied by the intranasal administration of CX-NP2 or free GH. The nontoxic behavior of the CX-NP2 NPs was tested by using hematoxylin and eosin (H&E) stained olfactory bulb sections compared to the negative control group (Fig. 4). In the negative control group, the six layers of the olfactory nerve, glomerular nerve, external plexiform, mitral cell, internal plexiform, and granular cell layer were visible, whereas those layers were visible even in the CX-NP2 treated group suggesting the nontoxic behavior of CX-NP2. Even though the authors do not mention the particle sizes to understand the BBB penetration, they confirmed the CX-NP2 significantly reduced the brain AChE level compared to the free GH treated group.

2.2.2. Synthetic polymeric NPs

Synthetic polymeric NPs are colloidal particles, which can be

further altered to tune the lipophilicity, charge, and biocompatibility during the synthetic process. [84] The high water solubility and cell permeability make polymeric NPs stable over a long period, even during the gradual release of the loaded drugs. Polymeric NPs have high drug loading capacity as well as low toxicity. Especially when they were coated with polyethylene glycol (PEG)-phospholipid copolymers, the toxicity could be reduced. Polyhydroxyalkanoates, polylactide-*co*-glycolide (PLGA), cyclodextrin-derived, and PEG-coated polymeric NPs are vastly applied as nanocarriers in brain-related studies whereas PLGA and PEGylated polymeric NPs are more common in AD treatment [67].

Polymeric NPs have been used in a vast range of AD-related pathogenesis, including Aβ and tau protein inhibition. Other than Aβ and tau related studies, polymeric NPs have been used to deliver the drug estradiol, which supports the replacement of the post-menopausal estrogen in women. Endogenous estrogen deficiency after menopause posed a risk of AD pathology development in women, knocking them down to a two-times' higher risk than men [85,86]. The post-menopausal estrogen replacement theory is another suggestion to reduce the probability of AD development in women [85]. Many clinical trials of estradiol oral consumption have been investigated to treat women with AD. However, on the contrary, the non-target specificity of the oral consumptions of estradiol has increased the risk of developing breast cancer by 30% [86]. Therefore, a targeted delivery system is essential to deliver the drug estradiol to the brain to minimize the adverse side effect of breast cancer development. Mittal et al. have designed a targeted nano-drug delivery system with tween 80 (T-80) coated PLGA polymeric NPs to deliver estradiol to the brain [87]. They stated that T-80 supports to cross the BBB by endocytosis. To be specific, the apolipoprotein E (Apo-E) or B (Apo-B) in the blood were adsorbed by T-80 coating onto the surface of PLGA NP resembling PLGA-NPs as low-density lipoproteins (LDL). As a result, the endocytic uptake of PLGA NPs occurred through LDL receptors of endothelial cells. The average particle size and zeta potential of the estradiol entrapped PLGA NPs were 134.7 nm and 68.5 mV, respectively. After increasing the T-80 coating percentage from 1 to 5%, the particle size has increased from 134.7 to 172. 4 nm. *In vitro* studies have shown that higher the T-80 coating percentage, higher the stability of the NPs in the simulated gastric and intestinal fluid. *In vivo* animal models suggested that a higher level of estradiol was observed in the brain after the oral administration of estradiol-encapsulated T-80 coated PLGA NPs than the uncoated NPs. The higher estradiol concentration in brain confirms the efficiency of the targeted delivery of T-80 coated PLGA NPs. Furthermore, the Aβ immunostaining results revealed that the oral administration of estradiol loaded PLGA NP was efficient as intramuscular free drug injection by confirming the prevention of peripheral drug burden effect, which enables the reduction of side effects.

Apart from the T-80 coated PLGA NPs which can adsorb Apo E and B, another polymeric NPs of PEG corona of poly (alkyl cyanoacrylate) (PACA) NPs also have identified as an excellent candidate to adsorb Apo-E making PACA another promising platform to bind with circulating $A\beta_{1\text{-}42}$ peptide in the blood [88]. In 2012, Brambilla et al. introduced a long-circulating PEG corona of PACA and poly (lactic acid) (PLA) NPs for the Aβ treatments [89]. Authors stated PLA and PACA NPs in PEG corona could interact with monomeric and soluble forms of $A\beta_{1\text{-}42}$. Even though the mean particle size was larger (110 nm), the results suggested the successful BBB penetration of the NPs by the strong adsorption of Apo-E onto NPs surface from the serum-supplemented with $A\beta_{1\text{-}42.}$ The Apo-E adsorption onto NPs increased the peptide affinity of NPs, which facilitates the successful elimination of Aβ from the serum. The authors further suggested that during the *in vivo* studies, the NPs acted like an "LDL-like" structure to clear the Aβ peptides from the serum while directing the soluble form of Aβ towards macrophages for destruction. Thus, the PEGylated NPs could probably prevent the Aβ aggregation in the brain via a sink effect mechanism.

Other than the LDL like structures that penetrate the BBB and bind to $A\beta_{1\text{-}42}$, in 2014, Zhang et al. reported a peptide conjugated biodegradable and low immunogenic polymeric NPs: Polyethylene glycol-poly lactic acid (PEG-PLA) NPs, which facilitate the BBB penetration and Aβ binding [90]. The PEG-PLA NPs have been conjugated to two peptides: D-enantiomeric peptide of QSH (QSHYRHISPAQV), which can bind and stain $A\beta_{1\text{-}42}$ at a sub-micromolar concentration, and a 12 amino acid peptide of TGN (TGNYKALHPHNG) which facilitates the BBB penetration. The mean particle size of NPs was 100 nm, and the zeta potential was approximate −20 mV. For the *in vitro* studies, the mouse brain endothelial cell lines of bEnd.3, which mimic the BBB, were used to test the BBB/cellular uptake. The results displayed a higher cellular uptake and the brain distribution of TGN-conjugated PEG-PLA NPs compared to the bare PEG-PLA NPs. The AD mouse models were produced by injecting $A\beta_{1\text{-}42}$ bilaterally into the hippocampus, and the efficiency of QSH peptide in diseased mouse models was tested by analyzing the accumulation of PEG-PLA NPs in the hippocampus. The experimental results revealed that the QSH administrated PEG-PLA NPs were efficient in clearing $A\beta_{1\text{-}42}$ peptides, making this bifunctional PEG-PLA NPs a good nanocarrier for AD treatment.

Along with the peptides, synthetic polymeric NPs have also been used in gene delivery studies to down-regulate BACE1. In 2016, Liu et al. proposed a Multi-purpose delivery system of gene and peptide along with PEGylated dendrigraft poly-L-lysine NPs for the down-regulation of β-site APP cleaving enzyme 1 (BACE1) [37]. BACE1 is the major β-secretase enzyme to convert APP into Aβ plaques through proteolytic cleavages [91]. Therefore, the downregulation of BACE1 could be one of the best resolutions to reduce the formation of Aβ plaques [91–93]. The most popular tool to knock down BACE1 antisense (BACE1-AS) gene is siRNA [94]. Due to the low stability of the siRNA in the blood circulation, Liu et al. used the BACE1-AS gene of shRNA, encoded with a plasmid that has loaded on PEGylated NPs [37,95]. Two peptides were conjugated to facilitate the BBB penetration and the inhibition of tau-related fibrils. The 29 amino acid peptide is the brain-targeting ligand, which was obtained from rabies virus glycoprotein (RVG29) that binds to n-acetylcholine receptors to facilitate the BBB penetration [96]. The D-peptide was used as the inhibitor for tau-related fibril formation that enables the delay or prevents the AD progression [97]. Then the shRNA was loaded onto NPs via the electrostatic attraction. Thus, Liu et al. have introduced multi-purpose nano-delivery for the AD treatment by loading dual-peptides and shRNA on the same PEGylated NPs (Fig. 5) [37].

The mean particle size of the gene and peptide conjugated NPs was 97 nm, and the zeta potential was 7.72 mV. The *in vitro* cytotoxicity and the cellular uptake were tested with SH-SY5Y cell lines, which express the nicotinic acetylcholine BBB receptors enabling the analysis of the receptor-mediated endocytosis of RVG29 peptide. The cell viability of the DGLs-PEG-RVG29-D-peptide/shBACE-As NPs was 80% at the concentration of 200 μg/mL, which proved the less cytotoxicity of the NPs. The *in vivo* images of C57BL/6 J mice were taken 1 h after the intravenous injection of the peptide and shRNA (shBACE-As) loaded NPs. The mice were injected with and without RVG29 peptide conjugated NPs. According to the *in vivo* and *ex vivo* images, the mice injected with RVG29 conjugated NPs have the most accumulation in the brain compared to the NPs without RVG29 (Fig. 6). Immunofluorescence study of mice suggested the AD brain has higher signals for BACE1 than the healthy brain. The BACE1 positive signals were diminished by DGLs-PEG-RVG29-D-peptide/shBACE-As and DGLs-PEG-RVG29/shBACE-As NPs, confirming the silencing and the downregulation of the BACE1 gene in the hippocampus region in AD mice. Further, the p-tau positive immunostaining studies revealed the D-peptide loaded NPs diminished p-tau positive signals in AD mice compared to the NPs without D-peptide, demonstrating the efficiency of the D-peptide. Therefore, the DGLs-PEG-RVG29-D-peptide/shBACE-As NPs were a better nano-delivery system for AD treatments.

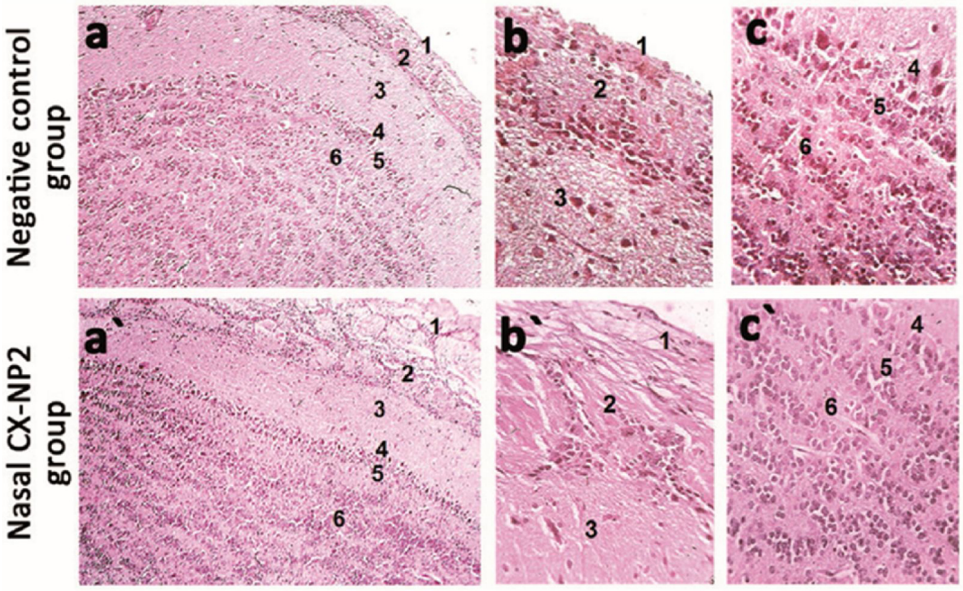

Fig. 4. The photomicrographs of H&E stained olfactory bulb sections of the negative control group (a–c), and intranasal administrated CX-NP2 group (a'-c'). The olfactory nerve, glomerular nerve, external plexiform, mitral cell, internal plexiform, and granular cell layer are the 1–6 layers denoted in the picture. Figure adapted from Ref. [83] with permissions from the publishers.

2.3. Metallic NPs

Metallic NPs can be synthesized basically from any metal and some metal oxides by obtaining different sizes, shapes, surface functionalization, structures, optical, and electronic properties [98,99]. Most commonly, silver, copper, gold, platinum, iron, and iron oxides (Fe_3O_4) are used as metallic NPs. Metallic NPs have remarkable physical and chemical properties that are different from the bulk materials, such as wavelength-dependent photoluminescence (PL), smaller size, high water dispersity, and localized surface plasmon resonance [99,100]. Vastly different fields use the benefits of metallic NPs such as electronic applications as catalysts, biomedical fields as nano-DDS *in vitro* and *in vivo,* and as enzymatic biosensors [98]. The biggest downside of the metallic NPs is the elevated toxicity at higher concentrations. There is a tendency to change the metallic NPs structure into toxic structures with the touch of chemicals in the synthesis process that ultimately leads to excrete and accumulate in the tissues during the *in vivo* applications, making it toxic to use for animal studies. However, gold NPs (AuNPs) and iron oxide NPs have been widely used as metallic NPs in AD studies.

2.3.1. Gold NPs

The most applicable metallic NP in every field is AuNP. AuNPs have drastic differences from its bulk material. Bulk gold is a yellow solid, which is inert, whereas the colloidal solution of AuNPs is wine red, which acts as an anti-oxidant [101]. AuNPs are more popular compared to other metal-based NPs because of its' unique properties such as shape, size-dependent optical properties, and low cytotoxicity. The size varies from 1 to 100 nm, and exhibit different shapes such as spherical, octahedral, decahedral, tetrahedral, triangles, and prisms [102]. AuNPs are more commonly used in biotechnology, biomedicine, and radiation medicine due to their ability to conjugate with probes and drugs [103,104]. Also, AuNPs are less cytotoxic, making them more prominent in drug delivery, including in brain targeted disease AD. The inhibition of Aβ fibril, tau protein, neurofibrillary tangle, and acetylcholine esterase have been studied with AuNPs [22,105–107]. However, AuNPs have been mostly used as biological colorimetric and fluorometric sensors as well as metal ion detectors to examine the AD pathogenesis.

Insoluble neurofibrillary tangle (NFT) formation in the brain is also one of the common AD pathologies. Neurofibrillary tangles are twisted fiber forms, appear due to the aggregation of hyperphosphorylated tau proteins in the brain. Tau protein phosphorylates rapidly and can be found in high concentrations in AD brains. Over time tau proteins bind to each other to form NFTs via "knots" [108–110]. Therefore, the importance of detecting the concentration level of tau protein is significant in understanding the NFTs level in the brain. In 2009, Neely et al. developed AuNPs-based two-photon Rayleigh scattering (TPRS) assay to detect the tau protein concentration by introducing the AuNPs as a colorimetric sensor [111]. The anti-tau antibody (tau-mab) conjugated AuNPs were used to identify tau proteins via the antibody-antigen interaction. Antibody-bound NPs, aggregate in the region of tau-proteins and bind to several antigen receptors because a single tau protein has several tau-mab antigen receptors. The reddish AuNPs have changed to blue when the antibody-bound NPs bound to the antigen receptor. The results have confirmed that the anti-tau antibody-conjugated AuNPs able to detect 1 pg/mL level of AD tau protein in the brain. The tau protein detection limit by antibody-bound NPs was two orders of magnitude lower than the cutoff value of tau-proteins (195 pg/mL) in cerebrospinal fluid, which reveals the ultra-sensitivity of the anti-tau antibody conjugated AuNPs. AuNPs have been used in AD studies, not only to identify the tau protein levels but also to examine the metal ion interaction with Aβ peptides. In 2010, Wang et al. developed a colorimetric sensor from AuNPs to analyze the interaction of the $A\beta_{1\text{-}16}$ peptide with metallic ions of Ca^{2+} and Zn^{2+} [112]. The molecular events of AuNPs can be easily observed qualitatively by its' color changes, which can be further analyzed analytically by the absorption spectrum and surface plasmon resonance (SPR). The main AD-related peptide $A\beta_{1\text{-}42}$ has 42 amino acids that undergo conformational changes into amyloid-like aggregates of $A\beta_{1\text{-}16,}$ which bind with metal ions to generate cell toxicity [113,114]. Therefore, Wang et al. synthesized $A\beta_{1\text{-}16}$ conjugated AuNPs to study the interaction with Ca^{2+} and Zn^{2+} [112]. The color of $A\beta_{1\text{-}16}$ bound AuNPs had changed from red to purple when it was interacted with Zn^{2+}. The SPR band was red-shifted from 527 to 537 nm, with the increment of Zn^{2+} concentration. Also, the results further confirmed that Ca^{2+} has a weak interaction with $A\beta_{1\text{-}16}$ bound AuNPs, displaying no change in SPR. The authors reported the $A\beta_{1\text{-}16}$ bound AuNPs are prominent sensors to detect the Ca^{2+} interactions.

Another colorimetric and fluorometric study has been developed by Liu et al. by using rhodamine B (RB) modified AuNPs as a sensor to detect the acetylcholinesterase (AChE) level in CSF [115]. The amino groups on RB were electrostatically attracted to negatively charged citrate-AuNPs displaying the fluorescence intensity quenching of RB

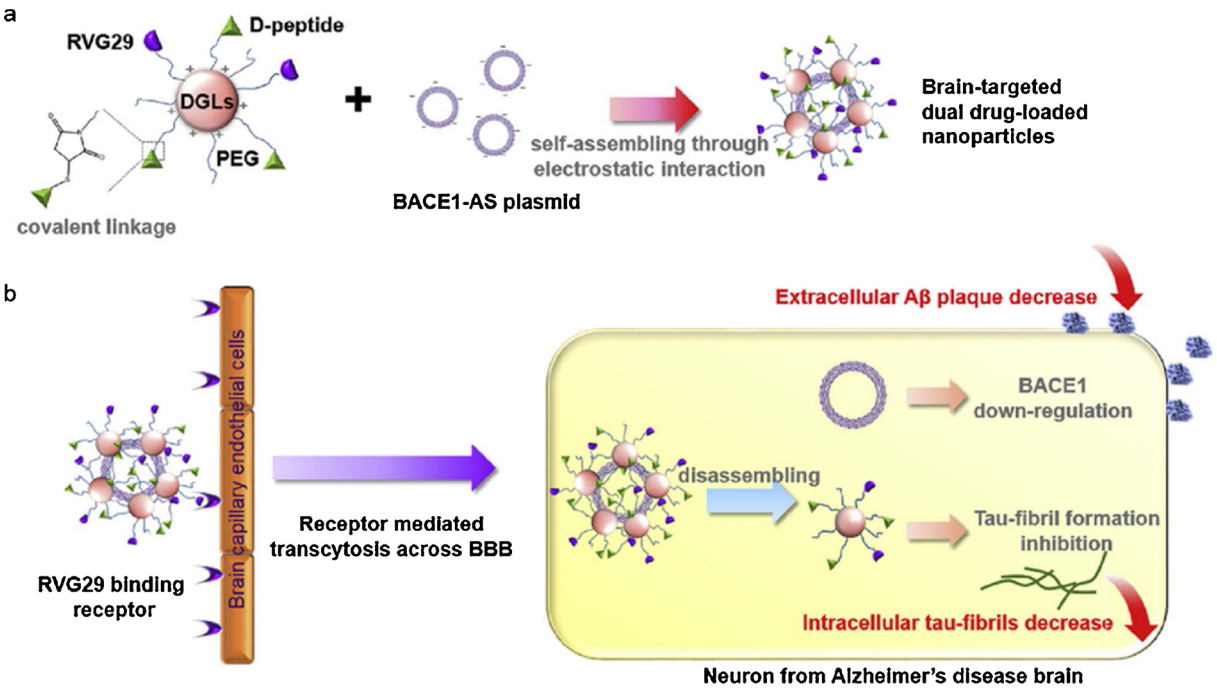

Fig. 5. Schematic diagram of a) the electrostatic attraction of the BACE1-AS plasmid, shRNA onto PEGylated NPs (DGLs), which has the covalently bound RVG29 and D-Peptide b) The intravenous administration of the NP system that crosses the BBB by RVG29 via the receptor-mediated transcytosis and then the dissembling of BACE1-AS and D-peptide in the brain [37]. Figure adapted from Ref [37]. with permissions from the publishers [37].

upon the interaction. After the addition of AChE and ATC to the medium, the AChE hydrolyzed ATC into thiocholine, which bound to AuNPs to form Au-S bond. Upon creating the Au-S bond, the AChE induced AuNP aggregation occurs, resulting in the desorption of RB from the AuNPs surface while increasing the fluorescence intensity (Fig. 7b). Therefore, the differences in fluorescence intensities of RB revealed the binding of AuNPs with thiocholine, which ultimately revealed the presence of AChE in the medium. The color of the RB-AuNPs changed from red to blue upon the introduction of AChE, whereas the AChE concentration increases the color turned to green by acting the RB-AuNPs as a colorimetric sensor. The UV–vis absorption spectra further showed the AChE induced AuNP aggregation. The RB-AuNP absorption peak at 520 nm has disappeared after introducing AChE to the medium while displaying the new two peaks at 600 and 800 nm, revealing the desorption of RB from the AuNP surface (Fig. 7 a). Also, the authors further stated the AChE detection limit by RB-AuNPs was much lower (0.1 mU mL^{-1}) than the previously reported values. Thus, the authors suggested that the RB-AuNPs assays could be useful to detect AChE levels in human AD brains.

However, as described above, Ray et al., and Wang and Liu et al., have only used AuNPs as sensors. AuNPs have also been used in quantitative AD studies, such as Aβ inhibitions. The inhibition of Aβ fibrillation and the initiation of its' alteration have been studied by Liao et al. by using bare AuNPs in the $A\beta_{1\text{-}40}$ peptide model system [116].

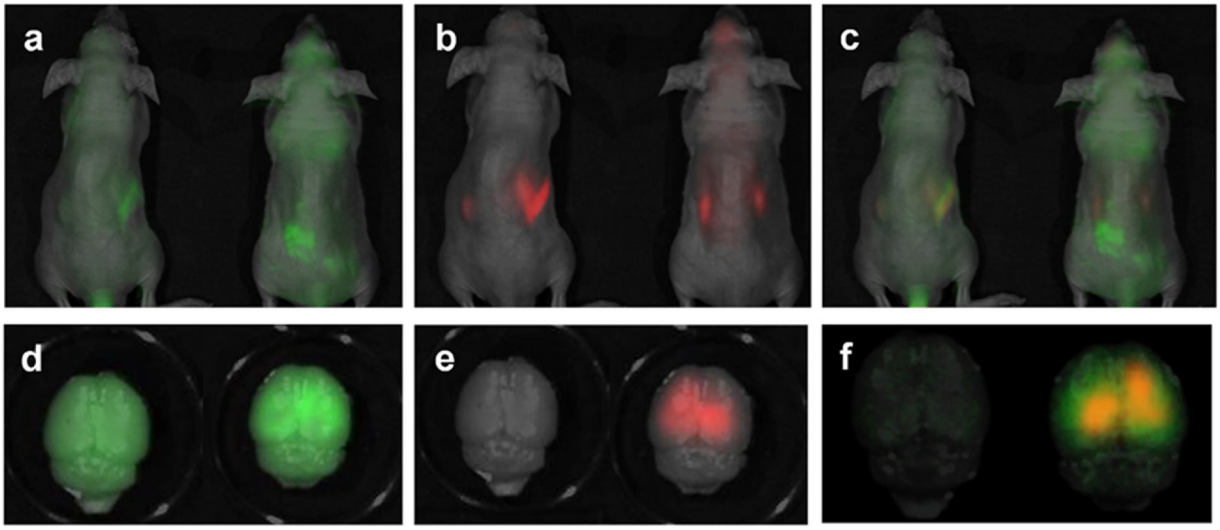

Fig. 6. The *in vivo* distribution of the NPs at 1 h post intravenous administration. The left mice are without RVG29, and right mice are with RVG29 containing NPs. a) Fluorescence image of YOYO-3-labeled DNA. b) Fluorescence image of IR-783-labeled D-peptide. c) Overlay image of YOYO and IR-783. d) Ex-vivo fluorescence image of the YOYO labeled brain (the left brain is the mice treated without RVG29, and the right brain is with RVG29 e). IR-783 tagged the D-peptide brain. f) Overlay the brain image of YOYO and IR-783. Figure reproduced from Ref. [37] with permissions from the publishers [37].

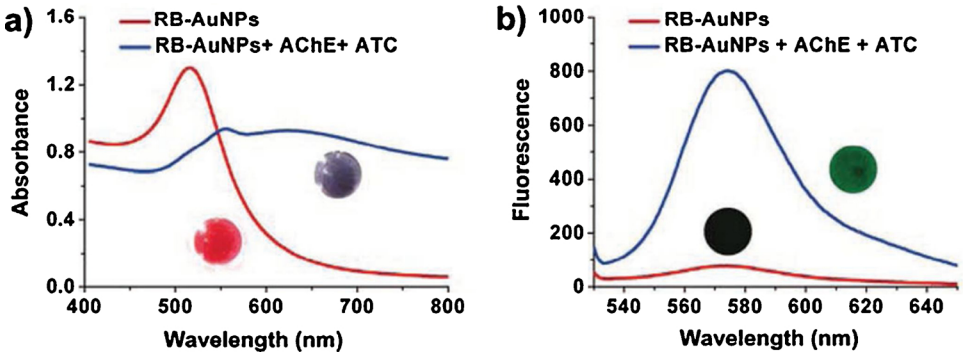

Fig. 7. a) The UV–vis absorption spectra show the color change of the RB-AuNP solution from red to purple b) The fluorescence intensity recovery upon the incubation of AChE and ATC along with RB-AuNPs. Figure adapted from Ref. [115] with permissions from the publishers (For interpretation of the references to color in this figure legend, the reader is referred to the web version of this article).

Negatively and positively charged AuNPs have been synthesized by conjugating carboxylic and amine groups, which have a mean particle size of 30 nm. The negatively charged NPs had a zeta potential of −39 mV and reported as less toxic, whereas amine-conjugated positively charged AuNPs (zeta potential of +7 mV) were reported as toxic. The negatively charged AuNPs have used to analyze the inhibition of Aβ fibrillation that has mainly affected in the elongation phase of the Aβ fibrillation rather than the nucleation during the inhibition process. Therefore, Liao et al. introduced negatively charged AuNPs as a prominent NP to be used in AD Aβ inhibition [116].

2.3.2. Magnetic NPs

In addition to AuNPs, some other metal-based NPs, such as iron, copper, and zinc, are used in AD treatments as metal-ion detection chelators. The widely used magnetic NP is Fe_3O_4 [117]. The magnetic NP of Fe_3O_4 has been commonly used in AD studies to detect the metal ions Cu^{2+} and Zn^{2+} that accelerate the ROS formation and Aβ aggregation.

In 2012 Li et al. have synthesized magnetic Fe_3O_4 caged NPs to use as a photolytic controlled release-prochelator (CQ) [118]. The photoactive molecules were covalently conjugated to the Fe_3O_4 caged NP surface, followed by the direct substitution of CQ molecules onto the surface. The loading quantity of the CQ molecules was calculated by thermogravimetric and elemental analyses. The relative immobilization efficiency was 56.96 μmol g^{-1} Fe_3O_4 NPs. The maximum release of the CQ molecules from the NPs surface was 30% at 3 min. The metal ion chelation of the photo-released product of CQ, with Cu^{2+}, was tested by UV–vis spectroscopy. CQ showed a peak at 335 nm in the UV–vis spectroscopic data, whereas after the Cu^{2+} addition, a new peak appeared at 410 nm corresponding to the copper complex. The controlled experiment was carried out in the dark, which shows no peak appeared at 410 nm, confirming the light-triggered release of CQ molecules. The effect of the photolytic product of CQ on Cu^{2+} induced Aβ aggregation was conducted in a weak acidic buffer solution, by based on the previous studies that have reported as the Cu^{2+} induced Aβ aggregation was more prominent at pH 6.6 [114,119]. Aβ aggregates were incubated with Fe_3O_4 NPs in dark or light irradiated conditions. Before the irradiation, the Aβ amorphous aggregates were 10–15 nm in size, while after the irradiation, fewer aggregates with smaller size were found. The samples incubated in the dark showed no change in the size of Aβ-metal aggregates. Therefore, the results concluded the effectiveness of light-sensitive magnetic NPs in inhibiting the Aβ aggregation.

Not only the Aβ cascade but the tracking of senile plaques is also equally important, and it was the first step of AD treatments in the early stages. However, the used pathological staining dyes, including chrysamine C, congo red, and styryl benzene, failed to cross BBB [120]. Therefore, alternatives should be created to stain the senile plaques or identify the plaque regions. In 2014, Zhou et al. have carried out a study related to the senile plaque staining process. They have synthesized a small hydrophobic lipophilic fluorescent probe of 1,1-dicyano-2-[-6-(dimethylamino) naphthalele-2-yl] propene (DDNP) carboxyl derivative, to cross the BBB and superparamagnetic NPs of Fe_3O_4 (SPIONPs) as a molecular imaging probe. [121] DDNP was incorporated into the SPIONPs through structural modification of carboxylic acid and succinic anhydride. The NPs were 11.7 nm in size, with a monodisperse size distribution. The *in vitro* binding affinity of the DDNP-SPIONPs to senile plaques was tested by fluorophotometry. Upon the binding of DDNP-SPIONPs to $Aβ_{1\text{-}40,}$ the fluorescence intensity was increased. The high viscous medium limited the intramolecular rotation of NPs which led the rigid structure to enhance the fluorescence quantum yield. The MR images show that the NP system has a 140.57 s^{-1} Fe mM^{-1} of MR relaxation property. Therefore, DDNP-SPIONP is an excellent candidate to bind with senile plaques and for the MRI studies that able to use as a contrasting agent as well as a good BBB crossing agent.

Besides using magnetic NPs as metal ion chelators or imaging probes, it was also used as tau protein detecting sensors. Most of the nanosensors have been developed to detect only β amyloids, not to identify the phosphorylated tau proteins. The clinical studies have shown that abnormally low levels of Aβ and tau proteins are present in early-stage AD brain plasma, indicating the need for ultra-sensitive probes [122–126]. Upon this need, Ray et al. have developed large scale chemically stable magnetic plasmonic nanoplatforms to separate and quantify the trace levels of β-amyloid and tau proteins in the whole blood samples [127]. The conjugation of magnetic Fe_3O_4 with gold plasmonic shell NPs was followed by the bioconjugation of the 2D graphene oxide. Furthermore, the hybrid graphene oxide was coated with amine-modified polyethylene glycol (HS-PEG) and conjugated with anti-amyloid and anti-tau antibodies. According to the ELISA experiment, the displayed high efficiencies for NP conjugated-anti-amyloid and anti-tau antibodies at the lowest concentration of 100 fg/mL are 98 and 97%, respectively. The authors further reported that this detection limit is lower than the regular ELISA kit detection of Aβ (0.312 ng/mL) and tau proteins (0.15 ng/mL), which makes their NP system is more sensitive to detect $Aβ_{1\text{-}42}$ and tau proteins.

So far, as described above, the most popular magnetic NP was Fe_3O_4 that has been used as metal ion detectors, imaging probes, and sensors. Besides Fe_3O_4 magnetic NP, ceria NP has also been used in AD-related studies as reactive oxygen species (ROS) scavengers. The ROS, such as superoxide anions, hydroxyl radicals, and hydrogen peroxides, cause mitochondrial dysfunction, contributing to AD pathogenesis [23,128]. ROS arise in the mitochondria as a byproduct of oxidative phosphorylation, and interact with Aβ peptides and the mitochondrial proteins of alcohol dehydrogenase, cyclophilin D, and ATP synthase to increase the Aβ production in the brain [129–132]. Therefore, the detection of ROS levels is equally vital as Aβ cascade in AD-related studies. In 2015, Kwon et al. synthesized triphenylphosphonium (TPP)-conjugated ceria NPs (TPP-ceria NPs) to use as ROS scavengers [24]. CeO_2 can reversibly bind to oxygen atoms, whereas the oxidation state can be changed from Ce^{3+} to Ce^{4+} on the NPs surface [133–135]. TPP is a lipophilic cation that can cross the negatively charged mitochondrial membrane, which makes it a mitochondrial-targeting ligand [136,137]. The *in vivo* studies

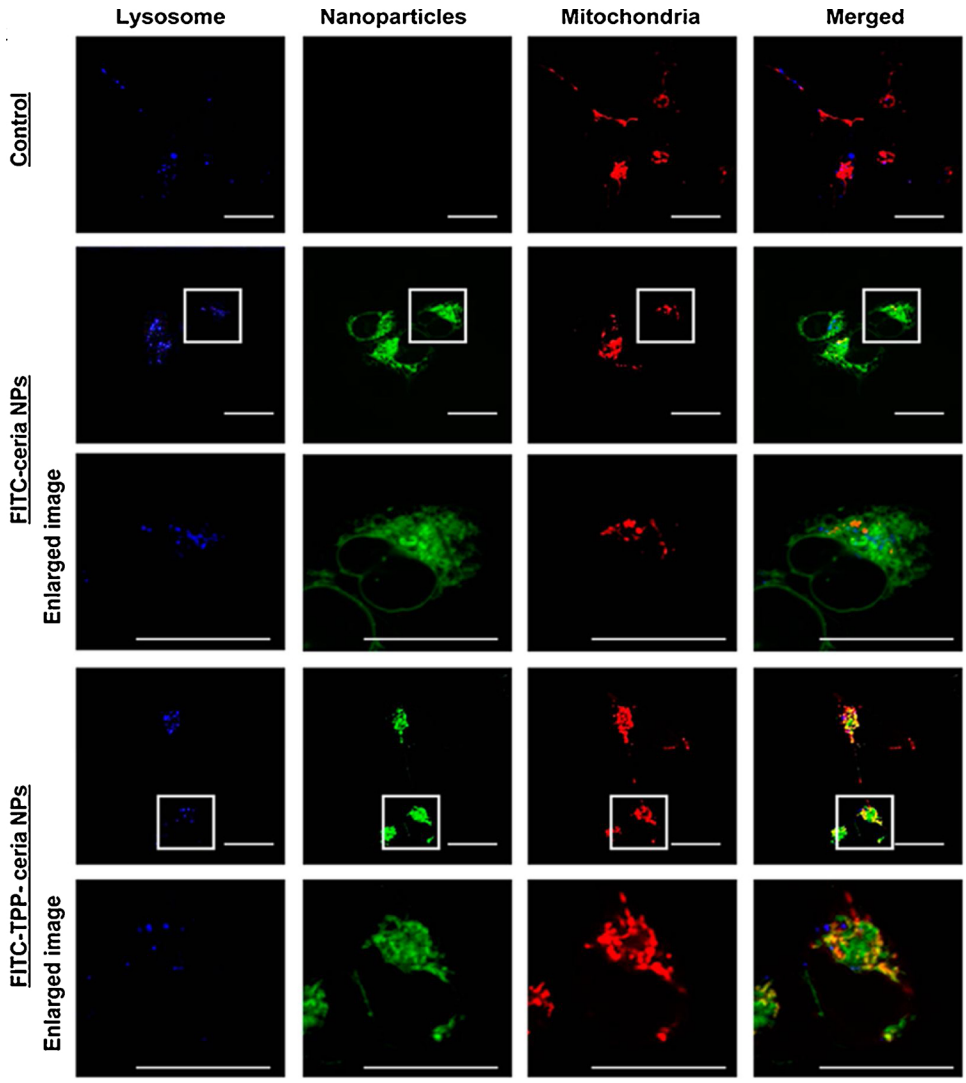

Fig. 8. The confocal fluorescence microscopic images of subcellular colocalization of FITC-labeled ceria NPs with and without TPP in SH-SY5Y cell lines. The control SH-SY5Y cells were stained with LysoTracker (blue) and MitoTracker (red). The enlarged areas in the square are shown in each image below. The colocalization of FITC-conjugated TPP-ceria/ceria NPs is shown in green. (Scale bar is 20 μm). Figure adapted from Ref. [24] with permissions from the publishers (For interpretation of the references to color in this figure legend, the reader is referred to the web version of this article).

of neuronal death suppression were tested with 5XFAD transgenic AD mice. The *in vitro* cytotoxicity studies have been conducted with human neuroblastoma SH-SY5Y cell lines, which displayed the low cytotoxicity for NPs. The hydrodynamic particle size of TPP-ceria NPs was approximately 57 nm. The cellular uptake was observed by the confocal fluorescence microscope using fluorescein isothiocyanate (FITC) labeled ceria NPs with and without TPP (Fig. 8). According to Fig. 8, the TPP-conjugated ceria NPs showed a higher cellular uptake than bare ceria NPs. The ROS scavenging activity was studied with the superoxide dismutase, and catalase activity assay by investigating the Aβ induced neuronal cell count. The reduction of the Aβ influenced neuronal cell loss was examined by the immunohistochemical analysis of NPs-treated 5XFAD mice. Their results suggested the TPP-ceria NPs are an effective neuroprotectant in the 5XFAD mice brain. However, the authors illustrated that the TPP-ceria NPs acted only as an anti-oxidant, which can scavenge the ROS but not as Aβ plaques eliminators.

2.4. Carbon-based NPs

Carbon nanotubes, fullerenes, graphene, and carbon dots (C-dots) are the most popular subunits in carbon-based NPs in drug delivery, whereas carbon nanotubes and carbon dots are most prominent in AD studies [138]. Carbon-based NPs were developed mainly as an alternative for toxic heavy metal-based NPs, such as quantum dots. Due to the non-toxicity, high biocompatibility, versatile surface functionality, and unique optical properties, carbon-based NPs have been widely used for *in vivo* deliveries [139].

2.4.1. Carbon nanotubes

Carbon nanotubes (CNTs) are fullerene allotropes that have long cylindrical shaped hollow structures. Based on the number of graphene sheets, they contain CNTs are categorized into two groups as single-walled (SWCNTs) and multi-walled (MWCNTs) nanotubes. CNT display astonishing features in thermal conductivity, optical, and electrical properties [140,141]. CNTs were used in nanomedicine in the early days because of the capability of interacting with mammalian cells and penetrate the cell membrane via cytoplasmic translocation. However, some studies have shown that CNTs are also toxic to human keratinocytes, kidney cells, T lymphocytes, and alveolar macrophages. Moreover, if inhaled, CNTs can even be toxic to the lungs [142,143].

Therefore, Yang et al. investigated the pharmacological and toxicological profile of SWCNTs to discover a method to use SWCNTs for drug delivery [144]. The toxicity of the SWCNTs was analyzed with lysosomes and mitochondria by analyzing the β-galactosidase secretion

levels. The higher levels of β-galactosidase indicate the damage of each organelle. The cytotoxicity studies of SWCNTs revealed that the ROS production was not induced in lysosomes but did in mitochondria. The authors further reported the β-galactosidase secretion was enhanced from three to eight times by SWCNTs with the presence of mitochondria, suggesting the SWCNTs cytotoxicity is majorly affecting the mitochondria. Moreover, Yang et al. have used SWCNTs to administrate Ach to the brain because SWCNTs can cross the BBB via nerve axon [144]. Also, due to the high affinity of SWCNTs to inorganic and organic molecules, the ACh molecules could easily load on SWCNT by the absorption through acetyl and quaternary ammonium group of ACh. The memory enhancement of SWCNT-ACh was tested with male AD mice, which were damaged by injecting neurotoxin, kainic acid, 24 h before the drug treatments. After treating the AD mice with SWCNT-ACh, the AD mice recovered the learning ability to the average level, whereas the bare ACh and bare SWCNTs treated groups have not displayed any recovery. The authors phrased, by keeping the SWCNT dosage below 300 mg/kg, the cytotoxicity towards mitochondria can be diminished. Therefore, Yang et al. claimed their SWCNT-ACh is a better candidate to recover the learning ability in AD mice while using SWCNT in a safe dosage [144].

Luo et al. have investigated the aggregation effect of SWCNTs with Aβ peptide and cross-β structures [145]. The conformational change of the random coiled Aβ peptide into the β sheet amyloid fibers has been identified as the primary mechanism in AD development. The CD spectrum data revealed, in the presence of SWCNTs, the conformational change of Aβ peptide into the β sheet is faster. However, the authors stated the SWCNTs promoted the nucleation at the low concentration of SWCNTs (0.0025 or 0.005 mg mL^{-1}), but at the higher concentration (0.1 mg mL^{-1}), the amyloid aggregation was inhibited. Luo et al. explained the above discrepancy by saying the SWCNTs fast bind to the Aβ peptides that have undergone the conformational change into parallel-β sheets, not to the cross-β sheets. After the binding of the SWCNTs to the parallel-β sheets, it slows down the conformational change into cross-β stacking, which eventually inhibits the amyloid aggregation [146,147]. However, the SWCNTs-interaction of Aβ is still not well understood.

In 2014, Xue et al. used SWCNTs to reverse the neuronal autophagy [148]. Autophagy is a lysosomal degradative pathway that damages organelle and neurons leading to neurodegenerative disorder AD [149,150]. Therefore, the main goal of Liang and co-workers is to investigate the upregulation of autophagy by using SWCNTs in a transgenic AD mouse model of CRND8 and wild type (WT) [148,151,152]. The carboxylic acid-functionalized, less cytotoxic SWCTs, has an average diameter of 1–2 nm. The CRND8 AD mouse models consist of an overexpressed human APP gene that contains two mutations. The overexpression of the APP gene induces the Aβ deposition while decreasing the lysosomal proteolysis. The reduction of lysosomal proteolysis causes amyloidogenesis increasing cognitive impairment [153]. Xue et al. discussed the mammalian target of Rapamycin (mTOR) induced autophagy [148]. The treatment of SWCNTs in CRND8 glia cells revealed that SWCNTs were capable of suppressing the autophagy induction, whereas in WT glia displayed a minimal effect. Therefore, the authors stated SWCNTs selectively reversed the APP-originated pathological action of mTOR signaling without affecting normal signaling in WT. Moreover, Liang and co-workers reported, SWCNTs not only reversed the autophagy induction caused by mTOR but also the weakening of lysosomal proteolysis, which leads to lysosomal swelling. Therefore, the autophagy was remarkably weakened by SWCNTs in primary glia in CRND8 mice while reversing the autophagic substrate clearance and autophagy dysfunction.

2.4.2. Carbon dots

Carbon dots (C-dots) are zero-dimensional nanomaterials that have unique optical properties [154–156]. C-dots can be synthesized via top-down or bottom-up approaches, which vary the optical and surface properties [157]. C-dots are tiny particles of 1–10 nm in size, which can be used in wider application range, especially in cell penetration studies [158,159]. The high photoluminescence, excitation wavelength-dependent or independent emission, tunable surface, high cell permeability, excellent biocompatibility, and nontoxicity, make C-dots excellent candidates for drug delivery in nanomedicine [39,160–162]. Although C-dots have been used widely in brain targeted tumor studies, the use in neurodegenerative studies, including AD, is deficient.

C-dots have been tested mainly in *in vitro* studies for identification and inhibition of the AChE activity and Aβ aggregation, but not in *in vivo*. Qian et al. developed a screening system to monitor and impede the AChE activity by using C-dots [163]. As described earlier in this review, the AChE enzyme maintains the level of Ach neurotransmitter by hydrolyzing Ach into thiocholine, which has a high affinity to copper (II) ion [163]. Qian et al. synthesized carboxylic functionalized C-dots, which yielded an intense green fluoresce, whereas when incorporated Cu^{2+} on the surface of C-dots, the fluorescence intensity was quenched [163,164]. Upon the addition of ACh and AChE to the C-dots-Cu^{2+} medium, AChE hydrolyzed Ach into thiocholine. Thiocholin was attracting Cu^{2+} from the C-dots surface, resulting in the fluorescence intensity recovery. Therefore, by monitoring the fluorescence intensity, the authors attempted to measure the AChE activity. Instead of pure thiocholine, the thiol products of L-Cysteine (Cys), L-homocysteine (Hcy), and glutathione (GSH) were used to analyze the quenching process of C-dots. The particle sizes of the bare C-dots in the dispersing medium were 2–5 nm, whereas after the addition of Cu^{2+}, the particle size increases up to 10 nm due to the aggregation. The authors reported that the 23.2 μM concentration of Cu^{2+} quenched C-dots fluorescence intensity nearly to the completeness wherein the addition of thiol compounds (which mimics the thiocholine) (333.3 μM) recovered up the intensity to 90%. The above results revealed the efficiency of monitoring the thiocholine by the C-dots-Cu^{2+} system. Moreover, the inhibition of AChE by tacrine was also analyzed by the fluorescent intensity. As the control experiment, the fluorescence intensity of C-dots-Cu^{2+} was measured without adding tacrine. In the presence of Cu^{2+} (10.4 μM), the fluorescence intensity of C-dots was quenched, while the addition of ACh and AChE, elevated the intensity up to 70% due to the production of thiocholine. However, the addition of tacrine to the medium did not induce fluorescence intensity confirming the inhibition of AChE by tacrine. Finally, the authors confirmed the effectiveness of screening AChE activity by C-dots in analytical methods, and they further reported this system could be expanded to use in biological analysis as well. In another study, Han et al. reported the efficiency of the C-dots in binding to Aβ monomers due to its high surface to volume ratio (Fig. 9) [165]. Moreover, Han et al. stated the C-dots inhibit the β-secretase (BACE1) enzyme by reducing the Aβ fibril formation [165]. The inhibition of BACE1 by C-dots was examined by fluorescence resonance energy transfer (FRET) assay. The authors reported that the BACE1 activity was inhibited at a higher concentration of C-dots, such as 10–20 μg/mL. They further elaborated that C-dots selectively bind to the active site of the BACE1 enzyme to inhibit the enzyme action. Moreover, Han et al. stated the C-dots were able to inhibit the early stages of Aβ monomers at a low concentration of 2 μg/mL. Also, the TEM measurements have further proved the binding of Aβ monomers to C-dots by displaying a 14 nm size for Aβ-C-dots conjugates and 6 nm for bare C-dots. However, 10 μg/mL of C-dots were not inhibiting the BACE1 activity in the presence of 10 μg/mL Aβ monomers. When the concentration of C-dots increased, the inhibition of BACE1 has been noticed. This behavior revealed that C-dots have a favorable predominant affinity towards Aβ monomers rather than into the BACE1 active site. The *in vivo* brain targeting delivery has been studied with an anesthetized zebrafish model. Transferrin was conjugated to facilitate BBB penetration. C-dots conjugates have crossed the BBB, and the confocal images revealed C-dots could target the forebrain of the zebrafish compared to dorsal and ventral sections. Therefore, the authors showed the efficiency of C-dots to cross the BBB while pre-dominantly

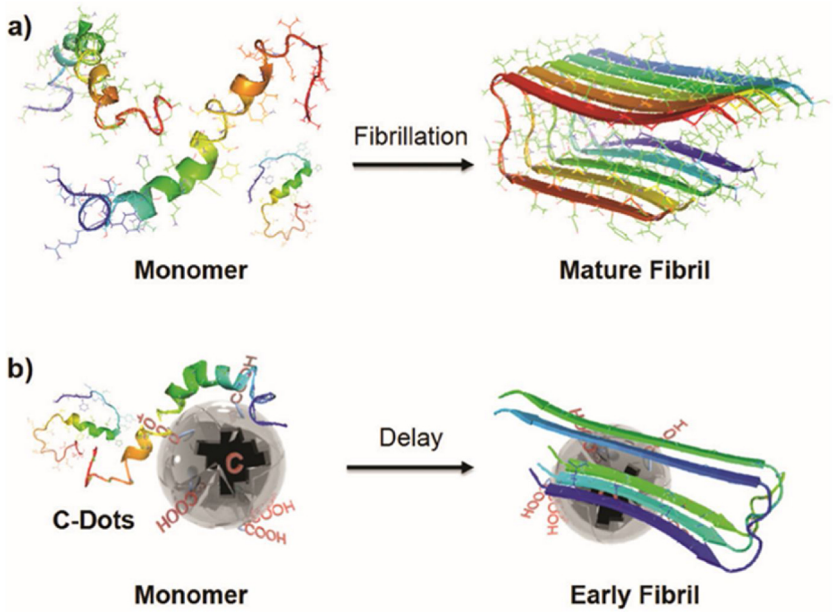

Fig. 9. Schematic diagram of a) Aβ fibrillation conformational change to mature fibrils b) the effect of inhibition of mature fibrils by C-dots. Figure reproduced from Ref. [165] with permissions from the publishers.

aiming Aβ monomers and at the higher concentration inhibiting the BACE 1.

2.5. Curcumin NPs

Curcumin is a natural polyphenolic antioxidant that scavenges superoxide and hydroxyl radicals. Commonly, it is known as an Indian and Chinese spice, *Curcuma longa* [166]. It has three significant curcuminoids of I, II, and III. Curcumin I (Curcumin) is the major curcuminoid which is commercially available up to 77%, whereas II (demethoxycurcumin) and III (bisdemethoxycurcumin) availabilities are 17 and 3%, respectively [167,168]. Structurewise, each curcuminoid has a diketone group that further tautomerized into the enol group. Studies have found that during the binding with Aβ, curcumin was found in enol structure [31]. Curcumin provides neuroprotection by activating the primary regulator of the antioxidant response, which is the transcription factor Nrf2 [169]. Further, curcumin has identified as an inhibitor for Aβ oligomerization and tau-phosphorylation and also as an inflammatory ROS scavenger and a neutralizer [170,171]. Even though curcumin is a potent neuroprotective agent, its' therapeutic efficacy is limited due to poor BBB/cell penetration, fast metabolism, and lack of bioavailability [36]. Therefore, the bioavailability must be increased to use curcumin as a therapeutic agent. Curcumin NPs and its NP-conjugates are the best possibilities to increase the bioavailability [172–175]. However, curcumin NPs are still under development, and not many experiments have been carried out for neurodegenerative disease AD.

In 2013, Cheng et al. synthesized curcumin NPs by encapsulating curcumin in PEG-PLA [35]. They used a multi-inlet vortex mixture (MIVM) to do a high energetic rapid NP precipitation while avoiding the nanoparticle aggregation. The average curcumin NPs sizes were approximately 55.2–66.2 nm, which were uniform even after one year of storage. The zeta potential was found to be −0.3 mV. *In vitro* studies were conducted with MDCK cell lines, mimicking BBB, and also expressing the multidrug resistance gene (MDR1). The transgenic mice Tg2576 have been used to perform the contextual fear conditioning (CFC) test. The results revealed that the oral administration of curcumin NPs significantly improve the memory of Tg2576 mouse models at a lower concentration of 23 mg/kg per week. Pharmacokinetic studies have shown the accumulation of curcumin NPs in the plasma and brain, 10–40 min s after the administration. The authors stated the higher concentration of NPs of less than 50 nm, were found at an elevated level in the brain at 10–40 min after the administration, which passed the BBB directly through tight junction. Whereas, the particles higher than 50 nm might enter the brain later, which were found after 80–160 min of administration. Therefore, curcumin NPs have displayed a more extended period of retention time in the brain compared to bulk curcumin revealing the higher bioavailability of the curcumin NPs.

3. Conclusion and viewpoints

Over the last era, AD diagnostic strategies and therapeutics usage via NPs have extensively been studied. As described above, although the Aβ cascade is considered the most prominent, the ROS, tau, and AChE levels are equally important. According to the experimental findings discussed above, the ambiguity of the disease is evident. There is no one particular reason for the disease; instead all the pathogenesis are inter-correlated, enhancing the severity of AD. Therefore, even though the experimental and clinical strategies demonstrated the effectiveness of the Np-based approaches, still the AD-related nano-deliveries should be optimized, especially in terms of lowering the side effects and acute toxicity, and enhancing the specificity of targeted delivery methods. Also, due to the indistinctness of AD, the most significant point in nano-drug delivery is to target multiple pathogeneses at the same time by loading numerous drugs on the same nano-vesicles.

All the NPs, we discussed here are biocompatible, and none/less toxic, except SWCNTs. SWCNTs are toxic to human keratinocytes, kidney cells, T lymphocytes, and alveolar macrophages, limiting the use of SWCNTs in nanodrug deliveries. Even though most of the other NPs are non-lethal, non-immunogenic, and less cytotoxic, the most significant downside is the larger particle size as BBB penetration favors the smaller particle size. Controversially, as discussed above in this review, liposomal and synthetic polymeric NPs are the largest NPs in size (> 100 nm) that have been used in many mouse models to prove the BBB penetration ability. However, the higher the particle size, the higher the tendency to damage the BBB endothelial cells in long-term usage. [176]

Moreover, the smaller particle size has a higher surface to volume ratio, which increases the drug loading capacity. Therefore, the particles such as chitosan, curcumin, and C-dots are more prominent to have

higher drug loading capacity due to their medium particle size (< 100 nm). However, the higher the molecular mass of chitosan NPs, the higher in degradability by dissatisfying long-term stability. Thus, concerning particle size and stability, C-dots are the promising nanocarriers that have an average particle size of 1–10 nm, which also favors multiple drug loading and higher loading capacity. Even though gold NPs have a larger average particle size than C-dots, both of the NPs have their unique optical properties that can be used in bioimaging. Besides, the higher drug loading capacity of smaller size NPs, the reduction of acute toxicity, can be achieved by using smaller size particles. The NPs which have larger particle sizes (> 100 nm) tend to aggregate, causing obstruct blood flaw and severe side effects of myocardial infarction, pulmonary embolism, and neurotoxicity. Therefore, using the smaller size NPs is equally vital to enhance the safer BBB penetration, reduction of the acute toxicity and side effects while having a higher drug loading capacity. [34] Thus far, C-dots can be designated as the promising NPs for BBB targeting deliveries due to their smaller size, low cytotoxicity, multiple drug loading capacity, and excitation wavelength-dependent/independent optical properties. Even though C-dots have been used in many tumor-targeting deliveries, including brain tumors, the tendency of employing them in AD-related studies are minimal. Therefore, C-dots might be a promising candidate for understanding AD pathogenesis and providing better therapeutics.

Author contribution

Sajini D. Hettiarachchi was mainly responsible for researching and compiling the data from the literature and conscripted the first draft of the manuscript (50%). Yiqun Zhou was critically edited and revised the manuscript (10%), whereas Elif Seven contributed by drawing the graphical abstract and revising the manuscript (5%). Madepalli K. Lakshmana, Ajeet K. Kaushik, and Hitendra S. Chand wrote the first half of the introduction while revising and editing the manuscript (15% in total). Roger M. Leblanc made the flow of the texts and critically reviewed and edited the manuscript (20%).

Declaration of Competing Interest

The authors declare no conflict of interest.

Acknowledgment

We greatly appreciate the generous funding support given by NSF grant GR-011298.

References

[1] M. Prince, R. Bryce, E. Albanese, A. Wimo, W. Ribeiro, C.P. Ferri, The global prevalence of dementia: a systematic review and metaanalysis, Alzheimers Dement. 9 (2013) 63–75.
[2] A. Wimo, M. Guerchet, G.-C. Ali, Y.-T. Wu, A.M. Prina, B. Winblad, L. Jönsson, Z. Liu, M. Prince, The worldwide costs of dementia 2015 and comparisons with 2010, Alzheimers Dement. 13 (2017) 1–7.
[3] C. Qiu, M. Kivipelto, E. von Strauss, Epidemiology of Alzheimer's disease: occurrence, determinants, and strategies toward intervention, Dialogues Clin. Neurosci. 11 (2009) 111–128.
[4] M.M. Corrada, R. Brookmeyer, A. Paganini-Hill, D. Berlau, C.H. Kawas, Dementia incidence continues to increase with age in the oldest old: the 90+ study, Ann. Neurol. 67 (2010) 114–121.
[5] D.J. Selkoe, Alzheimer's disease: genes, proteins, and therapy, Physiol. Rev. 81 (2001) 741–766.
[6] C.L. Masters, R. Bateman, K. Blennow, C.C. Rowe, R.A. Sperling, J.L. Cummings, Alzheimer's disease, Nat. Rev. Dis. Primers 1 (2015) 15056–15073.
[7] D.J. Selkoe, J. Hardy, The amyloid hypothesis of Alzheimer's disease at 25 years, EMBO Mol. Med. 8 (2016) 595–608.
[8] R. Joel, C. Jeffrey, H. John, S. Kory, A.D. Robert, Neurobiology of Alzheimer's disease: integrated molecular, physiological, anatomical, biomarker, and cognitive dimensions, Curr. Alzheimer Res. 12 (2015) 712–722.
[9] R.D. Terry, E. Masliah, D.P. Salmon, N. Butters, R. DeTeresa, R. Hill, L.A. Hansen, R. Katzman, Physical basis of cognitive alterations in Alzheimer's disease: synapse loss is the major correlate of cognitive impairment, Ann. Neurol. 30 (1991) 572–580.
[10] W. Samuel, E. Masliah, L.R. Hill, N. Butters, R. Terry, Hippocampal connectivity and Alzheimer's dementia, effects of synapse loss and tangle frequency in a two-component model, Neurology 44 (1994) 2081–2088.
[11] S.T. DeKosky, S.W. Scheff, Synapse loss in frontal cortex biopsies in Alzheimer's disease: correlation with cognitive severity, Ann. Neurol. 27 (1990) 457–464.
[12] R. Mayeux, Y. Stern, Epidemiology of Alzheimer disease, Cold Spring Harb. Perspect. Med. 2 (2012) a006239–a006256.
[13] B.C. Riedel, P.M. Thompson, R.D. Brinton, Age, APOE and sex: triad of risk of Alzheimer's disease, J. Steroid Biochem. Mol. Biol. 160 (2016) 134–147.
[14] C.M. Karch, A.M. Goate, Alzheimer's disease risk genes and mechanisms of disease pathogenesis, Biol. Psychiatry 77 (2015) 43–51.
[15] M. Rezazadeh, H. Hosseinzadeh, M. Moradi, B. Salek Esfahani, S. Talebian, S. Parvin, J. Gharesouran, Genetic discoveries and advances in late-onset Alzheimer's disease, J. Cell. Physiol. 234 (2019) 16873–16884.
[16] L. Shen, J. Jia, An overview of genome-wide association studies in Alzheimer's disease, Neurosci. Bull. 32 (2016) 183–190.
[17] R.J. O'Brien, P.C. Wong, Amyloid precursor protein processing and Alzheimer's disease, Annu. Rev. Neurosci. 34 (2011) 185–204.
[18] K. Buerger, M. Ewers, T. Pirttilä, R. Zinkowski, I. Alafuzoff, S.J. Teipel, J. DeBernardis, D. Kerkman, C. McCulloch, H. Soininen, H. Hampel, CSF phosphorylated tau protein correlates with neocortical neurofibrillary pathology in Alzheimer's disease, Brain 129 (2006) 3035–3041.
[19] S. Gauthier, B. Reisberg, M. Zaudig, R.C. Petersen, K. Ritchie, K. Broich, S. Belleville, H. Brodaty, D. Bennett, H. Chertkow, J.L. Cummings, M. de Leon, H. Feldman, M. Ganguli, H. Hampel, P. Scheltens, M.C. Tierney, P. Whitehouse, B. Winblad, Mild cognitive impairment, Lancet 367 (2006) 1262–1270.
[20] M. Sarter, M.E. Hasselmo, J.P. Bruno, B. Givens, Unraveling the attentional functions of cortical cholinergic inputs: interactions between signal-driven and cognitive modulation of signal detection, Brain Res. Rev. 48 (2005) 98–111.
[21] K. Herholz, Acetylcholine esterase activity in mild cognitive impairment and Alzheimer's disease, Eur. J. Nucl. Med. Mol. Imaging 35 (2008) 25–29.
[22] P. Shi, M. Li, J. Ren, X. Qu, Gold nanocage-based dual responsive "caged metal chelator" Release system: noninvasive remote control with near infrared for potential treatment of Alzheimer's disease, Adv. Funct. Mater. 23 (2013) 5412–5419.
[23] M.G. Bartley, K. Marquardt, D. Kirchhof, H.M. Wilkins, D. Patterson, D.A. Linseman, Overexpression of amyloid-β protein precursor induces mitochondrial oxidative stress and activates the intrinsic apoptotic cascade, J. Alzheimers Dis. 28 (2012) 855–868.
[24] H.J. Kwon, M.-Y. Cha, D. Kim, D.K. Kim, M. Soh, K. Shin, T. Hyeon, I. Mook-Jung, Mitochondria-targeting ceria nanoparticles as antioxidants for Alzheimer's disease, ACS Nano 10 (2016) 2860–2870.
[25] G. Aliev, J. Liu, J.C. Shenk, K. Fischbach, G.J. Pacheco, S.G. Chen, M.E. Obrenovich, W.F. Ward, A.G. Richardson, M.A. Smith, E. Gasimov, G. Perry, B.N. Ames, Neuronal mitochondrial amelioration by feeding acetyl-L-carnitine and lipoic acid to aged rats, J. Cell. Mol. Med. 13 (2009) 320–333.
[26] G. Aliev, H.H. Palacios, B. Walrafen, A.E. Lipsitt, M.E. Obrenovich, L. Morales, Brain mitochondria as a primary target in the development of treatment strategies for Alzheimer disease, Int. J. Biochem. Cell Biol. 41 (2009) 1989–2004.
[27] M. Mohsenzadegan, A. Mirshafiey, The immunopathogenic role of reactive oxygen species in Alzheimer disease, Iran. J. Allergy Asthma Immunol. 11 (2012) 203–216.
[28] J.M. Long, D.M. Holtzman, Alzheimer disease: an update on pathobiology and treatment strategies, Cell 179 (2019) 312–339.
[29] J. Sangyun, Molecular and cellular basis of neurodegeneration in Alzheimer's disease, Mol. Cells 40 (2017) 613–620.
[30] C. Zhang, A. Browne, D. Child, R.E. Tanzi, Curcumin decreases amyloid-β peptide levels by attenuating the maturation of amyloid-β precursor protein, J. Biol. Chem. 285 (2010) 28472–28480.
[31] D. Yanagisawa, N. Shirai, T. Amatsubo, H. Taguchi, K. Hirao, M. Urushitani, S. Morikawa, T. Inubushi, M. Kato, F. Kato, K. Morino, H. Kimura, I. Nakano, C. Yoshida, T. Okada, M. Sano, Y. Wada, K.-n. Wada, A. Yamamoto, I. Tooyama, Relationship between the tautomeric structures of curcumin derivatives and their Aβ-binding activities in the context of therapies for Alzheimer's disease, Biomaterials 31 (2010) 4179–4185.
[32] J.C. Carroll, E.R. Rosario, A. Villamagna, C.J. Pike, Continuous and cyclic progesterone differentially interact with estradiol in the regulation of Alzheimer-like pathology in female 3× transgenic-Alzheimer's disease mice, Endocrinology 151 (2010) 2713–2722.
[33] M.I. Fernández-Bachiller, C. Pérez, N.E. Campillo, J.A. Páez, G.C. González-Muñoz, P. Usán, E. García-Palomero, M.G. López, M. Villarroya, A.G. García, A. Martínez, M.I. Rodríguez-Franco, Tacrine–melatonin hybrids as multifunctional agents for Alzheimer's disease, with cholinergic, antioxidant, and neuroprotective properties, ChemMedChem 4 (2009) 828–841.
[34] Y. Zhou, Z. Peng, E.S. Seven, R.M. Leblanc, Crossing the blood-brain barrier with nanoparticles, J. Control. Release 270 (2018) 290–303.
[35] K.K. Cheng, C.F. Yeung, S.W. Ho, S.F. Chow, A.H. Chow, L. Baum, Highly stabilized curcumin nanoparticles tested in an *in vitro* blood-brain barrier model and in Alzheimer's disease Tg2576 mice, AAPS J. 15 (2013) 324–336.
[36] Y.-M. Tsai, C.-F. Chien, L.-C. Lin, T.-H. Tsai, Curcumin and its nano-formulation: the kinetics of tissue distribution and blood-brain barrier penetration, Int. J. Pharm. 416 (2011) 331–338.
[37] Y. Liu, S. An, J. Li, Y. Kuang, X. He, Y. Guo, H. Ma, Y. Zhang, B. Ji, C. Jiang, Brain-targeted co-delivery of therapeutic gene and peptide by multifunctional nanoparticles in Alzheimer's disease mice, Biomaterials 80 (2016) 33–45.
[38] S. Hettiarachchi, R. Graham, K. Mintz, Y. Zhou, S. Vanni, Z. Peng, R. Leblanc,

Triple conjugated carbon dots as a nano-drug delivery model for glioblastoma brain tumors, Nanoscale 11 (2019) 6192–6205.
[39] S. Li, D. Amat, Z. Peng, S. Vanni, S. Raskin, G. De Angulo, A.M. Othman, R.M. Graham, R.M. Leblanc, Transferrin conjugated nontoxic carbon dots for doxorubicin delivery to target pediatric brain tumor cells, Nanoscale 8 (2016) 16662–16669.
[40] X. Wang, L. Yang, Z. Chen, D.M. Shin, Application of nanotechnology in cancer therapy and imaging, CA Cancer J. Clin. 58 (2008) 97–110.
[41] M.Y. Hanafi-Bojd, M.R. Jaafari, N. Ramezanian, M. Xue, M. Amin, N. Shahtahmassebi, B. Malaekeh-Nikouei, Surface functionalized mesoporous silica nanoparticles as an effective carrier for epirubicin delivery to cancer cells, Eur. J. Pharm. Biopharm. 89 (2015) 248–258.
[42] D. Peer, J.M. Karp, S. Hong, O.C. Farokhzad, R. Margalit, R. Langer, Nanocarriers as an emerging platform for cancer therapy, Nat. Nanotechnol. 2 (2007) 751–760.
[43] R. Cheng, F. Meng, C. Deng, H.-A. Klok, Z. Zhong, Dual and multi-stimuli responsive polymeric nanoparticles for programmed site-specific drug delivery, Biomaterials 34 (2013) 3647–3657.
[44] V. Torchilin, Tumor delivery of macromolecular drugs based on the EPR effect, Adv. Drug Deliv. Rev. 63 (2011) 131–135.
[45] J. Gong, M. Chen, Y. Zheng, S. Wang, Y. Wang, Polymeric micelles drug delivery system in oncology, J. Control. Release 159 (2012) 312–323.
[46] K. Khosravi-Darani, A. Pardakhty, H. Honarpisheh, V.M. Rao, M.R. Mozafari, The role of high-resolution imaging in the evaluation of nanosystems for bioactive encapsulation and targeted nanotherapy, Micron 38 (2007) 804–818.
[47] M. Mehrabi, P. Esmaeilpour, A. Akbarzadeh, Z. Saffari, M. Farahnak, A. Farhangi, M. Chiani, Efficacy of pegylated liposomal etoposide nanoparticles on breast cancer cell lines, Turk. J. Med. Sci. 46 (2016) 567–571.
[48] D. Siegel, B. Tenchov, Influence of the lamellar phase unbinding energy on the relative stability of lamellar and inverted cubic phases, Biophys. J. 94 (2008) 3987–3995.
[49] Y. Panahi, M. Farshbaf, M. Mohammadhosseini, M. Mirahadi, R. Khalilov, S. Saghfi, A. Akbarzadeh, Recent advances on liposomal nanoparticles: synthesis, characterization and biomedical applications, Artif. Cells Nanomed. Biotechnol. 45 (2017) 788–799.
[50] A.K. Thompson, M.R. Mozafari, H. Singh, The properties of liposomes produced from milk fat globule membrane material using different techniques, Le lait 87 (2007) 349–360.
[51] H.T. Nasrabadi, E. Abbasi, S. Davaran, M. Kouhi, A. Akbarzadeh, Bimetallic nanoparticles: preparation, properties, and biomedical applications, Artif. Cells Nanomed. Biotechnol. 44 (2016) 376–380.
[52] M. Sanchez-Purra, V. Ramos, V. Petrenko, V. Torchilin, S. Borros, Double-targeted polymersomes and liposomes for multiple barrier crossing, Int. J. Pharm. 511 (2016) 946–956.
[53] R.P. Singh, G. Sharma, L. Kumari, B. Koch, S. Singh, S. Bharti, P.S. Rajinikanth, B.L. Pandey, M.S. Muthu, RGD-TPGS decorated theranostic liposomes for brain targeted delivery, Colloids Surf. B Biointerfaces 147 (2016) 129–141.
[54] Y. Luo, Z. Liu, X. Zhang, J. Huang, X. Yu, J. Li, D. Xiong, X. Sun, Z. Zhong, Effect of a controlled-release drug delivery system made of oleanolic acid formulated into multivesicular liposomes on hepatocellular carcinoma *in vitro* and *in vivo*, Int. J. Nanomed. Nanosurg. 11 (2016) 3111–3129.
[55] H. Daraee, A. Eatemadi, E. Abbasi, S. Fekri Aval, M. Kouhi, A. Akbarzadeh, Application of gold nanoparticles in biomedical and drug delivery, Artif. Cells Nanomed. Biotechnol. 44 (2016) 410–422.
[56] M. Gobbi, F. Re, M. Canovi, M. Beeg, M. Gregori, S. Sesana, S. Sonnino, D. Brogioli, C. Musicanti, P. Gasco, M. Salmona, M.E. Masserini, Lipid-based nanoparticles with high binding affinity for amyloid-β1–42 peptide, Biomaterials 31 (2010) 6519–6529.
[57] K. Matsuzaki, Physicochemical interactions of amyloid β-peptide with lipid bilayers, Biochim. Biophys. Acta 1768 (2007) 1935–1942.
[58] M.-S. Lin, H.-M. Chiu, F.-J. Fan, H.-T. Tsai, S.S.-S. Wang, Y. Chang, W.-Y. Chen, Kinetics and enthalpy measurements of interaction between β-amyloid and liposomes by surface plasmon resonance and isothermal titration microcalorimetry, Colloids Surf. B Biointerfaces 58 (2007) 231–236.
[59] C. Balducci, S. Mancini, S. Minniti, P. La Vitola, M. Zotti, G. Sancini, M. Mauri, A. Cagnotto, L. Colombo, F. Fiordaliso, E. Grigoli, M. Salmona, A. Snellman, M. Haaparanta-Solin, G. Forloni, M. Masserini, F. Re, Multifunctional liposomes reduce brain β-amyloid burden and ameliorate memory impairment in Alzheimer's disease mouse models, J. Neurosci. 34 (2014) 14022–14031.
[60] S. Mancini, S. Minniti, M. Gregori, G. Sancini, A. Cagnotto, P.-O. Couraud, L. Ordóñez-Gutiérrez, F. Wandosell, M. Salmona, F. Re, The hunt for brain Aβ oligomers by peripherally circulating multi-functional nanoparticles: potential therapeutic approach for Alzheimer disease, Nanomedicine 12 (2016) 43–52.
[61] E.A. Tanifum, I. Dasgupta, M. Srivastava, R.C. Bhavane, L. Sun, J. Berridge, H. Pourgarzham, R. Kamath, G. Espinosa, S.C. Cook, J.L. Eriksen, A. Annapragada, Intravenous delivery of targeted liposomes to amyloid-β pathology in APP/PSEN1 transgenic mice, PLoS One 7 (2012) e48515–e48528.
[62] A. Lockhart, Imaging Alzheimer's disease pathology: one target, many ligands, Drug Discov. Today 11 (2006) 1093–1099.
[63] E.A. Tanifum, K. Ghaghada, C. Vollert, E. Head, J.L. Eriksen, A. Annapragada, A novel liposomal nanoparticle for the imaging of amyloid plaque by magnetic resonance imaging, J. Alzheimers Dis. 52 (2016) 731–745.
[64] X. Zheng, X. Shao, C. Zhang, Y. Tan, Q. Liu, X. Wan, Q. Zhang, S. Xu, X. Jiang, Intranasal H102 peptide-loaded liposomes for brain delivery to treat Alzheimer's disease, Pharm. Res. 32 (2015) 3837–3849.
[65] L. Zhang, F. Gu, J. Chan, A. Wang, R. Langer, O. Farokhzad, Nanoparticles in medicine: therapeutic applications and developments, Clin. Pharmacol. Ther. 83 (2008) 761–769.
[66] J.P. Rao, K.E. Geckeler, Polymer nanoparticles: preparation techniques and size-control parameters, Prog. Polym. Sci. 36 (2011) 887–913.
[67] F. Masood, Polymeric nanoparticles for targeted drug delivery system for cancer therapy, Mater. Sci. Eng. C 60 (2016) 569–578.
[68] A. Kumari, S.K. Yadav, S.C. Yadav, Biodegradable polymeric nanoparticles based drug delivery systems, Colloids Surf. B Biointerfaces 75 (2010) 1–18.
[69] S. Hajji, I. Younes, O. Ghorbel-Bellaaj, R. Hajji, M. Rinaudo, M. Nasri, K. Jellouli, Structural differences between chitin and chitosan extracted from three different marine sources, Int. J. Biol. Macromol. 65 (2014) 298–306.
[70] I. Zainol, S. Ghani, A. Mastor, M. Derman, M. Yahya, Enzymatic degradation study of porous chitosan membrane, Mater. Res. Innov. 13 (2009) 316–319.
[71] J. Sarvaiya, Y. Agrawal, Chitosan as a suitable nanocarrier material for anti-Alzheimer drug delivery, Int. J. Biol. Macromol. 72 (2015) 454–465.
[72] H.-C. Yang, M.-H. Hon, The effect of the molecular weight of chitosan nanoparticles and its application on drug delivery, Microchem. J. 92 (2009) 87–91.
[73] P. Taşkın, H. Canısağ, M. Şen, The effect of degree of deacetylation on the radiation induced degradation of chitosan, Radiat. Phys. Chem. 94 (2014) 236–239.
[74] J.P. Nance, K.M. Vannella, D. Worth, C. David, D. Carter, S. Noor, C. Hubeau, L. Fitz, T.E. Lane, T.A. Wynn, E.H. Wilson, Chitinase dependent control of protozoan cyst burden in the brain, PLoS Pathog. 8 (2012) e1002990–e1003005.
[75] M. Watabe-Rudolph, Z. Song, L. Lausser, C. Schnack, Y. Begus-Nahrmann, M.-O. Scheithauer, G. Rettinger, M. Otto, H. Tumani, D. Thal, J. Attems, K.A. Jellinger, H.A. Kestler, C.A.F. von Arnim, K.L. Rudolph, Chitinase enzyme activity in CSF is a powerful biomarker of Alzheimer disease, Neurology 78 (2012) 569–577.
[76] A. Kumar, S. Dogra, A. Prakash, Neuroprotective effects of Centella asiatica against intracerebroventricular colchicine-induced cognitive impairment and oxidative stress, Int. J. Alzheimers Dis. 2009 (2009) 972178–972185.
[77] B. Wilson, M.K. Samanta, K. Santhi, K.P.S. Kumar, M. Ramasamy, B. Suresh, Significant delivery of tacrine into the brain using magnetic chitosan microparticles for treating Alzheimer's disease, J. Neurosci. Methods 177 (2009) 427–433.
[78] B. Wilson, M.K. Samanta, K. Santhi, K.S. Kumar, M. Ramasamy, B. Suresh, Chitosan nanoparticles as a new delivery system for the anti-Alzheimer drug tacrine, Nanomedicine 6 (2010) 144–152.
[79] Y.S. Elnaggar, S.M. Etman, D.A. Abdelmonsif, O.Y. Abdallah, Intranasal piperine-loaded chitosan nanoparticles as brain-targeted therapy in Alzheimer's disease: optimization, biological efficacy, and potential toxicity, J. Pharm. Sci. 104 (2015) 3544–3556.
[80] K.T. Dineley, A.A. Pandya, J.L. Yakel, Nicotinic ACh receptors as therapeutic targets in CNS disorders, Trends Pharmacol. Sci. 36 (2015) 96–108.
[81] S. Bhattacharya, C. Haertel, A. Maelicke, D. Montag, Galantamine slows down plaque formation and behavioral decline in the 5XFAD mouse model of Alzheimer's disease, PLoS One 9 (2014) e89454–e89465.
[82] A.K. Leonard, A.P. Sileno, G.C. Brandt, C.A. Foerder, S.C. Quay, H.R. Costantino, *In vitro* formulation optimization of intranasal galantamine leading to enhanced bioavailability and reduced emetic response *in vivo*, Int. J. Pharm. 335 (2007) 138–146.
[83] A.S. Hanafy, R.M. Farid, M.W. Helmy, S.S. ElGamal, Pharmacological, toxicological and neuronal localization assessment of galantamine/chitosan complex nanoparticles in rats: future potential contribution in Alzheimer's disease management, Drug Deliv. 23 (2016) 3111–3122.
[84] A.Z. Wang, R. Langer, O.C. Farokhzad, Nanoparticle delivery of cancer drugs, Annu. Rev. Med. 63 (2012) 185–198.
[85] L.A. Craig, N.S. Hong, J. Kopp, R.J. McDonald, Cholinergic depletion of the medial septum followed by phase shifting does not impair memory or rest–activity rhythms measured under standard light/dark conditions in rats, Brain Res. Bull. 79 (2009) 53–62.
[86] N. Bodor, P. Buchwald, Brain-targeted delivery of estradiol, Am. J. Drug Deliv. 4 (2006) 161–175.
[87] G. Mittal, H. Carswell, R. Brett, S. Currie, M.R. Kumar, Development and evaluation of polymer nanoparticles for oral delivery of estradiol to rat brain in a model of Alzheimer's pathology, J. Control. Release 150 (2011) 220–228.
[88] H.R. Kim, K. Andrieux, S. Gil, M. Taverna, H. Chacun, D. Desmaële, F. Taran, D. Georgin, P. Couvreur, Translocation of poly (ethylene glycol-co-hexadecyl) cyanoacrylate nanoparticles into rat brain endothelial cells: role of apolipoproteins in receptor-mediated endocytosis, Biomacromolecules 8 (2007) 793–799.
[89] D. Brambilla, R. Verpillot, B. Le Droumaguet, J. Nicolas, M. Taverna, J. Kóňa, B. Lettiero, S.H. Hashemi, L. De Kimpe, M. Canovi, M. Gobbi, V. Nicolas, W. Scheper, S.M. Moghimi, I. Tvaroška, P. Couvreur, K. Andrieux, PEGylated nanoparticles bind to and alter amyloid-beta peptide conformation: toward engineering of functional nanomedicines for Alzheimer's disease, ACS Nano 6 (2012) 5897–5908.
[90] C. Zhang, X. Wan, X. Zheng, X. Shao, Q. Liu, Q. Zhang, Y. Qian, Dual-functional nanoparticles targeting amyloid plaques in the brains of Alzheimer's disease mice, Biomaterials 35 (2014) 456–465.
[91] Y. Jiang, K.A. Mullaney, C.M. Peterhoff, S. Che, S.D. Schmidt, A. Boyer-Boiteau, S.D. Ginsberg, A.M. Cataldo, P.M. Mathews, R.A. Nixon, Alzheimer's-related endosome dysfunction in Down syndrome is Aβ-independent but requires APP and is reversed by BACE-1 inhibition, Proc. Natl. Acad. Sci. U. S. A. 107 (2010) 1630–1635.
[92] I. Hussain, J. Hawkins, D. Harrison, C. Hille, G. Wayne, L. Cutler, T. Buck, D. Walter, E. Demont, C. Howes, A. Naylor, P. Jeffrey, M.I. Gonzalez, C. Dingwall, A. Michel, S. Redshaw, J.B. Davis, Oral administration of a potent and selective non-peptidic BACE-1 inhibitor decreases β-cleavage of amyloid precursor protein

and amyloid-β production in vivo, J. Neurochem. 100 (2007) 802–809.
[93] N. Charrier, B. Clarke, L. Cutler, E. Demont, C. Dingwall, R. Dunsdon, P. East, J. Hawkins, C. Howes, I. Hussain, P. Jeffrey, G. Maile, R. Matico, J. Mosley, A. Naylor, A. O'Brien, S. Redshaw, P. Rowland, V. Soleil, K.J. Smith, S. Sweitzer, P. Theobald, D. Vesey, D.S. Walter, G. Wayne, Second generation of hydroxyethylamine BACE-1 inhibitors: optimizing potency and oral bioavailability, J. Med. Chem. 51 (2008) 3313–3317.
[94] M.A. Faghihi, F. Modarresi, A.M. Khalil, D.E. Wood, B.G. Sahagan, T.E. Morgan, C.E. Finch, G.S. Laurent III, P.J. Kenny, C. Wahlestedt, Expression of a noncoding RNA is elevated in Alzheimer's disease and drives rapid feed-forward regulation of β-secretase, Nat. Med. 14 (2008) 723–730.
[95] Y. Gao, L. Chen, Z. Zhang, Y. Chen, Y. Li, Reversal of multidrug resistance by reduction-sensitive linear cationic click polymer/iMDR1-pDNA complex nanoparticles, Biomaterials 32 (2011) 1738–1747.
[96] P. Kumar, H. Wu, J.L. McBride, K.-E. Jung, M.H. Kim, B.L. Davidson, S.K. Lee, P. Shankar, N. Manjunath, Transvascular delivery of small interfering RNA to the central nervous system, Nature 448 (2007) 39–43.
[97] K.R. Brunden, J.Q. Trojanowski, V.M.-Y. Lee, Advances in tau-focused drug discovery for Alzheimer's disease and related tauopathies, Nat. Rev. Drug Discov. 8 (2009) 783–793.
[98] B. Mordorski, A. Friedman, Chapter 4 - metal nanoparticles for microbial infection, in: R. Boukherroub, S. Szunerits, D. Drider (Eds.), Functionalized Nanomaterials for the Management of Microbial Infection, Elsevier, Boston, 2017, pp. 77–109.
[99] Y. Dahman, Nanotechnology and Functional Materials for Engineers, Elsevier, 2017, pp. 2–3.
[100] J. Chen, H. Javaheri, B. Al-Chikh Sulaiman, Y. Dahman, Chapter 1 - synthesis, characterization and applications of nanoparticles, in: A.M. Grumezescu (Ed.), Fabrication and Self-Assembly of Nanobiomaterials, William Andrew Publishing, 2016, pp. 1–27.
[101] A. Khan, R. Rashid, G. Murtaza, A. Zahra, Gold nanoparticles: synthesis and applications in drug delivery, Trop. J. Pharm. Res. 13 (2014) 1169–1177.
[102] A. Kumar, B.M. Boruah, X.-J. Liang, Gold nanoparticles: promising nanomaterials for the diagnosis of cancer and HIV/AIDS, J. Nanomater. 2011 (2011) 17–33.
[103] S. Tedesco, H. Doyle, J. Blasco, G. Redmond, D. Sheehan, Oxidative stress and toxicity of gold nanoparticles in Mytilus edulis, Aquat. Toxicol. 100 (2010) 178–186.
[104] M. Ganeshkumar, T.P. Sastry, M.S. Kumar, M.G. Dinesh, S. Kannappan, L. Suguna, Sun light mediated synthesis of gold nanoparticles as carrier for 6-mercaptopurine: preparation, characterization and toxicity studies in zebrafish embryo model, Mater. Res. Bull. 47 (2012) 2113–2119.
[105] R.C. Triulzi, Q. Dai, J. Zou, R.M. Leblanc, Q. Gu, J. Orbulescu, Q. Huo, Photothermal ablation of amyloid aggregates by gold nanoparticles, Colloids Surf. B Biointerfaces 63 (2008) 200–208.
[106] J. Geng, K. Qu, J. Ren, X. Qu, Rapid and efficient screening of Alzheimer's disease β-amyloid inhibitors using label-free gold nanoparticles, Mol. Biosyst. 6 (2010) 2389–2391.
[107] N. Gao, H. Sun, K. Dong, J. Ren, X. Qu, Gold-nanoparticle-based multifunctional amyloid-β inhibitor against Alzheimer's disease, Chem. Eur. J. 21 (2015) 829–835.
[108] R. Brookmeyer, E. Johnson, K. Ziegler-Graham, H.M. Arrighi, Forecasting the global burden of Alzheimer's disease, Alzheimers Dement. 3 (2007) 186–191.
[109] G. Bu, Apolipoprotein E and its receptors in Alzheimer's disease: pathways, pathogenesis and therapy, Nat. Rev. Neurosci. 10 (2009) 333–344.
[110] L. Bertram, R.E. Tanzi, Thirty years of Alzheimer's disease genetics: the implications of systematic meta-analyses, Nat. Rev. Neurosci. 9 (2008) 768–778.
[111] A. Neely, C. Perry, B. Varisli, A.K. Singh, T. Arbneshi, D. Senapati, J.R. Kalluri, P.C. Ray, Ultrasensitive and highly selective detection of Alzheimer's disease biomarker using two-photon Rayleigh scattering properties of gold nanoparticle, ACS Nano 3 (2009) 2834–2840.
[112] C. Wang, J. Wang, D. Liu, Z. Wang, Gold nanoparticle-based colorimetric sensor for studying the interactions of β-amyloid peptide with metallic ions, Talanta 80 (2010) 1626–1631.
[113] K. Pagel, T. Seri, H. von Berlepsch, J. Griebel, R. Kirmse, C. Böttcher, B. Koksch, How metal ions affect amyloid formation: Cu^{2+}-and Zn^{2+}-sensitive peptides, ChemBioChem 9 (2008) 531–536.
[114] H. Yu, J. Ren, X. Qu, Different hydration changes accompanying copper and zinc binding to amyloid β-peptide: water contribution to metal binding, ChemBioChem 9 (2008) 879–882.
[115] D. Liu, W. Chen, Y. Tian, S. He, W. Zheng, J. Sun, Z. Wang, X. Jiang, A highly sensitive gold-nanoparticle-based assay for acetylcholinesterase in cerebrospinal fluid of transgenic mice with Alzheimer's disease, Adv. Healthc. Mater. 1 (2012) 90–95.
[116] Y.H. Liao, Y.J. Chang, Y. Yoshiike, Y.C. Chang, Y.R. Chen, Negatively charged gold nanoparticles inhibit Alzheimer's amyloid-β fibrillization, induce fibril dissociation, and mitigate neurotoxicity, Small 8 (2012) 3631–3639.
[117] F.U. Amin, A.K. Hoshiar, T.D. Do, Y. Noh, S.A. Shah, M.S. Khan, J. Yoon, M.O. Kim, Osmotin-loaded magnetic nanoparticles with electromagnetic guidance for the treatment of Alzheimer's disease, Nanoscale 9 (2017) 10619–10632.
[118] M. Li, Z. Liu, J. Ren, X. Qu, Inhibition of metal-induced amyloid aggregation using light-responsive magnetic nanoparticle prochelator conjugates, Chem. Sci. 3 (2012) 868–873.
[119] B. Raman, T. Ban, K.-i. Yamaguchi, M. Sakai, T. Kawai, H. Naiki, Y. Goto, Metal ion-dependent effects of clioquinol on the fibril growth of an amyloid β peptide, J. Biol. Chem. 280 (2005) 16157–16162.
[120] S. Vallabhajosula, 18F-labeled positron emission tomographic radiopharmaceuticals in oncology: an overview of radiochemistry and mechanisms of tumor localization, Semin. Nucl. Med. Lung Scan Update 37 (2007) 400–419.
[121] J. Zhou, H. Fa, W. Yin, J. Zhang, C. Hou, D. Huo, D. Zhang, H. Zhang, Synthesis of superparamagnetic iron oxide nanoparticles coated with a DDNP-carboxyl derivative for *in vitro* magnetic resonance imaging of Alzheimer's disease, Mater. Sci. Eng. C 37 (2014) 348–355.
[122] K. Blennow, H. Hampel, M. Weiner, H. Zetterberg, Cerebrospinal fluid and plasma biomarkers in Alzheimer disease, Nat. Rev. Neurol. 6 (2010) 131–144.
[123] M. Mapstone, A.K. Cheema, M.S. Fiandaca, X. Zhong, T.R. Mhyre, L.H. MacArthur, W.J. Hall, S.G. Fisher, D.R. Peterson, J.M. Haley, M.D. Nazar, S.A. Rich, D.J. Berlau, C.B. Peltz, M.T. Tan, C.H. Kawas, H.J. Federoff, Plasma phospholipids identify antecedent memory impairment in older adults, Nat. Med. 20 (2014) 415–421.
[124] H. Amiri, K. Saeidi, P. Borhani, A. Manafirad, M. Ghavami, V. Zerbi, Alzheimer's disease: pathophysiology and applications of magnetic nanoparticles as MRI theranostic agents, ACS Chem. Neurosci. 4 (2013) 1417–1429.
[125] K.P. Kepp, Bioinorganic chemistry of Alzheimer's disease, Chem. Rev. 112 (2012) 5193–5239.
[126] M. Paulite, C. Blum, T. Schmid, L. Opilik, K. Eyer, G.C. Walker, R. Zenobi, Full spectroscopic tip-enhanced Raman imaging of single nanotapes formed from β-amyloid (1–40) peptide fragments, ACS Nano 7 (2013) 911–920.
[127] T. Demeritte, B.P. Viraka Nellore, R. Kanchanapally, S.S. Sinha, A. Pramanik, S.R. Chavva, P.C. Ray, Hybrid graphene oxide based plasmonic-magnetic multifunctional nanoplatform for selective separation and label-free identification of Alzheimer's disease biomarkers, ACS Appl. Mater. Interfaces 7 (2015) 13693–13700.
[128] T. Nakamura, S.A. Lipton, Redox regulation of mitochondrial fission, protein misfolding, synaptic damage, and neuronal cell death: potential implications for Alzheimer's and Parkinson's diseases, Apoptosis 15 (2010) 1354–1363.
[129] A. Federico, E. Cardaioli, P. Da Pozzo, P. Formichi, G.N. Gallus, E. Radi, Mitochondria, oxidative stress and neurodegeneration, J. Neurol. Sci. 322 (2012) 254–262.
[130] J. Yun, T. Finkel, Mitohormesis, Cell Metab. 19 (2014) 757–766.
[131] H. Du, L. Guo, F. Fang, D. Chen, A.A. Sosunov, G.M. McKhann, Y. Yan, C. Wang, H. Zhang, J.D. Molkentin, F.J. Gunn-Moore, J.P. Vonsattel, O. Arancio, J.X. Chen, S.D. Yan, Cyclophilin D deficiency attenuates mitochondrial and neuronal perturbation and ameliorates learning and memory in Alzheimer's disease, Nat. Med. 14 (2008) 1097–1105.
[132] C. Schmidt, E. Lepsverdize, S. Chi, A. Das, S. Pizzo, A. Dityatev, M. Schachner, Amyloid precursor protein and amyloid β-peptide bind to ATP synthase and regulate its activity at the surface of neural cells, Mol. Psychiatry 13 (2008) 953–969.
[133] A. Karakoti, S. Singh, J.M. Dowding, S. Seal, W.T. Self, Redox-active radical scavenging nanomaterials, Chem. Soc. Rev. 39 (2010) 4422–4432.
[134] I. Celardo, J.Z. Pedersen, E. Traversa, L. Ghibelli, Pharmacological potential of cerium oxide nanoparticles, Nanoscale 3 (2011) 1411–1420.
[135] A.S. Karakoti, S. Singh, A. Kumar, M. Malinska, S.V. Kuchibhatla, K. Wozniak, W.T. Self, S. Seal, PEGylated nanoceria as radical scavenger with tunable redox chemistry, J. Am. Chem. Soc. 131 (2009) 14144–14145.
[136] S. Marrache, S. Dhar, Engineering of blended nanoparticle platform for delivery of mitochondria-acting therapeutics, Proc. Natl. Acad. Sci. U. S. A. 109 (2012) 16288–16293.
[137] S. Biswas, N.S. Dodwadkar, P.P. Deshpande, V.P. Torchilin, Liposomes loaded with paclitaxel and modified with novel triphenylphosphonium-PEG-PE conjugate possess low toxicity, target mitochondria and demonstrate enhanced antitumor effects *in vitro* and *in vivo*, J. Control. Release 159 (2012) 393–402.
[138] S. Augustine, J. Singh, M. Srivastava, M. Sharma, A. Das, B.D. Malhotra, Recent advances in carbon based nanosystems for cancer theranostics, Biomater. Sci. 5 (2017) 901–952.
[139] Q.-L. Yan, M. Gozin, F.-Q. Zhao, A. Cohen, S.-P. Pang, Highly energetic compositions based on functionalized carbon nanomaterials, Nanoscale 8 (2016) 4799–4851.
[140] M. Swierczewska, K.Y. Choi, E.L. Mertz, X. Huang, F. Zhang, L. Zhu, H.Y. Yoon, J.H. Park, A. Bhirde, S. Lee, A facile, one-step nanocarbon functionalization for biomedical applications, Nano Lett. 12 (2012) 3613–3620.
[141] Y. Weizmann, D.M. Chenoweth, T.M. Swager, Addressable terminally linked DNA-CNT nanowires, J. Am. Chem. Soc. 132 (2010) 14009–14011.
[142] J.G. Rouse, J. Yang, A.R. Barron, N.A. Monteiro-Riviere, Fullerene-based amino acid nanoparticle interactions with human epidermal keratinocytes, Toxicol. In Vitro 20 (2006) 1313–1320.
[143] M. Bottini, S. Bruckner, K. Nika, N. Bottini, S. Bellucci, A. Magrini, A. Bergamaschi, T. Mustelin, Multi-walled carbon nanotubes induce T lymphocyte apoptosis, Toxicol. Lett. 160 (2006) 121–126.
[144] Z. Yang, Y. Zhang, Y. Yang, L. Sun, D. Han, H. Li, C. Wang, Pharmacological and toxicological target organelles and safe use of single-walled carbon nanotubes as drug carriers in treating Alzheimer disease, Nanomedicine 6 (2010) 427–441.
[145] J. Luo, S.K. Wärmländer, C.-H. Yu, A. Gräslund, J.P. Abrahams, The Aβ peptide forms non-amyloid fibrils in the presence of carbon nanotubes, Nanoscale 6 (2014) 6720–6726.
[146] Y. Raz, Y. Miller, Interactions between Aβ and mutated Tau lead to polymorphism and induce aggregation of Aβ-mutated tau oligomeric complexes, PLoS One 8 (2013) e73303–e73316.
[147] Y. Miller, B. Ma, R. Nussinov, Synergistic interactions between repeats in tau protein and Aβ amyloids may be responsible for accelerated aggregation via polymorphic states, Biochemistry 50 (2011) 5172–5181.
[148] X. Xue, L.-R. Wang, Y. Sato, Y. Jiang, M. Berg, D.-S. Yang, R.A. Nixon, X.-J. Liang, Single-walled carbon nanotubes alleviate autophagic/lysosomal defects in primary glia from a mouse model of Alzheimer's disease, Nano Lett. 14 (2014) 5110–5117.
[149] R.A. Nixon, The role of autophagy in neurodegenerative disease, Nat. Med. 19

(2013) 983–997.
[150] W.E. Hochfeld, S. Lee, D.C. Rubinsztein, Therapeutic induction of autophagy to modulate neurodegenerative disease progression, Acta Pharmacol. Sin. 34 (2013) 600–604.
[151] H.J. Lee, J. Park, O.J. Yoon, H.W. Kim, D.H. Kim, W.B. Lee, N.-E. Lee, J.V. Bonventre, S.S. Kim, Amine-modified single-walled carbon nanotubes protect neurons from injury in a rat stroke model, Nat. Nanotechnol. 6 (2011) 121–125.
[152] S. Bari, P.P.Y. Chu, A. Lim, X. Fan, F.P.H. Gay, R.M. Bunte, T.K.H. Lim, S. Li, G.N.C. Chiu, W.Y.K. Hwang, Protective role of functionalized single walled carbon nanotubes enhance ex vivo expansion of hematopoietic stem and progenitor cells in human umbilical cord blood, Nanomedicine 9 (2013) 1304–1316.
[153] D.-S. Yang, P. Stavrides, P.S. Mohan, S. Kaushik, A. Kumar, M. Ohno, S.D. Schmidt, D. Wesson, U. Bandyopadhyay, Y. Jiang, M. Pawlik, C.M. Peterhoff, A.J. Yang, D.A. Wilson, P. St George-Hyslop, D. Westaway, P.M. Mathews, E. Levy, A.M. Cuervo, R.A. Nixon, Reversal of autophagy dysfunction in the TgCRND8 mouse model of Alzheimer's disease ameliorates amyloid pathologies and memory deficits, Brain 134 (2010) 258–277.
[154] X. Han, S. Li, Z. Peng, A.O. Al-Yuobi, A.S. Omar Bashammakh, M.S. El-Shahawi, R.M. Leblanc, Interactions between carbon nanomaterials and biomolecules, J. Oleo Sci. 65 (2016) 1–7.
[155] Z. Peng, X. Han, S. Li, A.O. Al-Youbi, A.S. Bashammakh, M.S. El-Shahawi, R.M. Leblanc, Carbon dots: biomacromolecule interaction, bioimaging and nanomedicine, Coord. Chem. Rev. 343 (2017) 256–277.
[156] S.-T. Yang, L. Cao, P.G. Luo, F. Lu, X. Wang, H. Wang, M.J. Meziani, Y. Liu, G. Qi, Y.-P. Sun, Carbon dots for optical imaging *in vivo*, J. Am. Chem. Soc. 131 (2009) 11308–11309.
[157] E.S. Seven, S.K. Sharma, D. Meziane, Y. Zhou, K.J. Mintz, R.R. Pandey, C.C. Chusuei, R.M. Leblanc, Close-packed langmuir monolayers of saccharide-based carbon dots at the rir-subphase interface, Langmuir 35 (2019) 6708–6718.
[158] I.P.-J. Lai, S.G. Harroun, S.-Y. Chen, B. Unnikrishnan, Y.-J. Li, C.-C. Huang, Solid-state synthesis of self-functional carbon quantum dots for detection of bacteria and tumor cells, Sens. Actuators B Chem. 228 (2016) 465–470.
[159] A. Zhao, Z. Chen, C. Zhao, N. Gao, J. Ren, X. Qu, Recent advances in bioapplications of C-dots, Carbon 85 (2015) 309–327.
[160] Y.-F. Wu, H.-C. Wu, C.-H. Kuan, C.-J. Lin, L.-W. Wang, C.-W. Chang, T.-W. Wang, Multi-functionalized carbon dots as theranostic nanoagent for gene delivery in lung cancer therapy, Sci. Rep. 6 (2016) 21170–21181.
[161] S. Li, Z. Peng, R.M. Leblanc, Method to determine protein concentration in the protein–nanoparticle conjugates aqueous solution using circular dichroism spectroscopy, Anal. Chem. 87 (2015) 6455–6459.
[162] L. Wu, M. Luderer, X. Yang, C. Swain, H. Zhang, K. Nelson, A.J. Stacy, B. Shen, G.M. Lanza, D. Pan, Surface passivation of carbon nanoparticles with branched macromolecules influences near infrared bioimaging, Theranostics 3 (2013) 677–686.
[163] Z.S. Qian, L.J. Chai, Y.Y. Huang, C. Tang, J.J. Shen, J.R. Chen, H. Feng, A real-time fluorescent assay for the detection of alkaline phosphatase activity based on carbon quantum dots, Biosens. Bioelectron. 68 (2015) 675–680.
[164] Z. Qian, L. Chai, C. Tang, Y. Huang, J. Chen, H. Feng, A fluorometric assay for acetylcholinesterase activity and inhibitor screening with carbon quantum dots, Sens. Actuators B Chem. 222 (2016) 879–886.
[165] X. Han, Z. Jing, W. Wu, B. Zou, Z. Peng, P. Ren, A. Wikramanayake, Z. Lu, R.M. Leblanc, Biocompatible and blood–brain barrier permeable carbon dots for inhibition of Aβ fibrillation and toxicity, and BACE1 activity, Nanoscale 9 (2017) 12862–12866.
[166] S. Mishra, K. Palanivelu, The effect of curcumin (turmeric) on Alzheimer's disease: an overview, Ann. Indian Acad. Neurol. 11 (2008) 13–19.
[167] E.V. Rao, P. Sudheer, Revisiting curcumin chemistry part I: a new strategy for the synthesis of curcuminoids, Indian J. Pharm. Sci. 73 (2011) 262–270.
[168] M. Chen, Z.-Y. Du, X. Zheng, D.-L. Li, R.-P. Zhou, K. Zhang, Use of curcumin in diagnosis, prevention, and treatment of Alzheimer's disease, Neural Regen. Res. 13 (2018) 742–752.
[169] C. Yang, X. Zhang, H. Fan, Y. Liu, Curcumin upregulates transcription factor Nrf2, HO-1 expression and protects rat brains against focal ischemia, Brain Res. 1282 (2009) 133–141.
[170] T. Ahmed, S. Enam, A. Gilani, Curcuminoids enhance memory in an amyloid-infused rat model of Alzheimer's disease, Neuroscience 169 (2010) 1296–1306.
[171] B. Ray, S. Bisht, A. Maitra, A. Maitra, D.K. Lahiri, Neuroprotective and neurorescue effects of a novel polymeric nanoparticle formulation of curcumin (NanoCurc™) in the neuronal cell culture and animal model: implications for Alzheimer's disease, J. Alzheimers Dis. 23 (2011) 61–77.
[172] A.V. Vergoni, G. Tosi, R. Tacchi, M.A. Vandelli, A. Bertolini, L. Costantino, Nanoparticles as drug delivery agents specific for CNS: *in vivo* biodistribution, Nanomedicine 5 (2009) 369–377.
[173] M.K. Reddy, V. Labhasetwar, Nanoparticle-mediated delivery of superoxide dismutase to the brain: an effective strategy to reduce ischemia-reperfusion injury, FASEB J. 23 (2009) 1384–1395.
[174] M.N. Tiwari, S. Agarwal, P. Bhatnagar, N.K. Singhal, S.K. Tiwari, P. Kumar, L.K.S. Chauhan, D.K. Patel, R.K. Chaturvedi, M.P. Singh, K.C. Gupta, Nicotine-encapsulated poly (lactic-co-glycolic) acid nanoparticles improve neuroprotective efficacy against MPTP-induced parkinsonism, Free Radic. Biol. Med. 65 (2013) 704–718.
[175] J.B. Hoppe, K. Coradini, R.L. Frozza, C.M. Oliveira, A.B. Meneghetti, A. Bernardi, E.S. Pires, R.C. Beck, C.G. Salbego, Free and nanoencapsulated curcumin suppress β-amyloid-induced cognitive impairments in rats: involvement of BDNF and Akt/GSK-3β signaling pathway, Neurobiol. Learn. Mem. 106 (2013) 134–144.
[176] J.K. Sahni, S. Doggui, J. Ali, S. Baboota, L. Dao, C. Ramassamy, Neurotherapeutic applications of nanoparticles in Alzheimer's disease, J. Control. Release 152 (2011) 208–231.